TNO innovation for life

KEM-19b Seismicity estimates for potential subsurface operations

Part 2

TNO Public › TNO 2025 R10452
20 June 2025

TNO 2025 R10452 – 20 June 2025

KEM-19b
Seismicity estimates for potential subsurface operations

Part 2

Author(s)	S.Osinga, P.Fokker, S. Bottero

Classification report	TNO Public
Title	TNO Public
Report text	TNO Public
Number of pages	44 (excl. front and back cover)
Number of appendices	0
Sponsor	The Dutch Ministry of Economic Affairs and Climate
Programme name	Kennisprogramma Effecten van Mijnbouw - KEM program

Managementsamenvatting

Dit rapport beschrijft onderzoek naar de aardbevingseffecten van mogelijke toekomstige geothermische operaties in de zuidwestelijke aquifer van het Groningen gasveld aan de hand van verschillende benaderingen.

Allereerst onderzoeken we de ruimtelijke variabiliteit in *seismiciteitsneiging* (d.w.z. de neiging van het systeem om aardbevingen te genereren als reactie op poriedruk- en temperatuurveranderingen) met behulp van het Groningen seismische bronmodel waarin compactie gerelateerd is aan seismische gebeurtenispercentages. We tonen aan dat het gebied met de hoogste seismiciteitsneiging zich net ten noorden van de stad Groningen bevindt en zijn positie in de loop van de tijd niet verandert. Deze relatief hoge seismiciteitsneiging is het gevolg van relatief lage poriedrukken en grote verticale spanningen in dit gebied, gecombineerd met de aanwezigheid van in kaart gebrachte breuken. Dit resultaat is algemeen toepasbaar en is niet afhankelijk van het operationele ontwerp van een specifiek geothermisch project.

Daarnaast onderzoeken we de ruimtelijke omvang en de grootte van spanningsveranderingen die gepaard gaan met druk- en temperatuurveranderingen als gevolg van typische geothermische operaties en hoe deze worden beïnvloed door poriedrukdaling voorafgaand aan de start van de geothermische operaties. Deze onderzoeken zijn van belang omdat de ZW-aquifer van het Groningen gasveld een daling van de poriedruk ervaart als gevolg van de historische gasproductie in het Groningen veld. De spanningsveranderingen bepalen of breuken kunnen worden geheractiveerd, wat hier wordt aangenomen als indicatief voor geïnduceerde seismische slip. Over het algemeen vinden we dat de belangrijkste thermo-elastische spanningsveranderingen geassocieerd zijn met het gekoelde volume van de aquifer gecentreerd rond de injector, tot 1,5 keer de straal van de gekoelde zone (d.w.z. de afstand van de injectieput tot de rand van het gekoelde reservoirvolume). Poro-elastische effecten zijn minder belangrijk in de context van de ZW-aquifer. Heractivering van breuken is ook voornamelijk geconcentreerd in deze gekoelde zone. Daarom is het belangrijk om zowel het gekoelde volume als de geometrie van breuken die kunnen worden geheractiveerd en seismogeen kunnen zijn, in kaart te brengen. De straal van het gekoelde reservoirvolume hangt af van het volume geïnjecteerd koud water, de hoogte van de permeabele zone en de thermische eigenschappen van de vloeistof en de rots. We stellen methoden voor om de gekoelde reservoirzone te monitoren, waaronder puttesten, pulstesten en DTS. De delen van de aquifer waar de poriedruk hoog zijn gebleven zijn doorgaans iets stabieler, minder vatbaar voor breukheractivering en dus minder seismogeen. Dit hangt echter af van de gekozen geomechanische parameters (specifiek de Poisson's ratio en de Biot-constante).

Ten slotte is het belangrijk om het verzet van een breuk te beoordelen wanneer deze aanwezig is in de gekoelde zone (of zone met verminderde poriedruk) van een geothermisch veld. Een verzet gelijk aan de dikte van de aquifer, waarbij de top van het hangend blok op dezelfde diepte ligt als de basis van het liggend blok, maximaliseert het effect van drukdaling en koeling op de geïnduceerde spanningen. Dit geldt alle mogelijke hellingen van de breuk.

Over het algemeen is het belangrijk om onzekerheden in invoerparameters mee te nemen in een projectspecifieke analyse van geothermische operaties. In deze studie worden een aantal

belangrijke invoerparameters geïdentificeerd: de oorspronkelijke in-situ spanningsstaat, de wrijvingskenmerken van de breuk, en elastische moduli.

Het hier beschreven werk heeft zich explicitet gericht op generieke resultaten die breed toepasbaar zijn op alle potentiële geothermische projecten en vormt geen directe input voor een specifiek project. Vanwege hun brede toepasbaarheid kunnen de resultaten van dit project echter dienen als belangrijke input voor studies gericht op dergelijke projecten.

Executive Summary

We investigate the effects on seismicity of potential future geothermal operations in the southwest (SW) aquifer of the Groningen gas field using a number of different approaches.

First, we investigate the spatial variability in *seismicity propensity* (i.e. the tendency of the system to generate earthquakes in response to pore pressure and temperature changes) utilizing the Groningen seismic source model framework in which compaction is related to seismic event rates. We show that the area with the highest seismicity propensity is just north of the city of Groningen and does not change its position through time. This relatively high seismicity propensity stems from relatively low pore pressures and large vertical strains in this area, combined with the presence of mapped faults. This result is generally applicable and does not depend on the operational design of any particular geothermal project.

Second, we investigate the spatial extent and magnitude of stress changes associated with pressure and temperature changes due to typical geothermal operations and how these are influenced by pore pressure decline prior to commencing the geothermal operations. These investigations are of interest since the SW aquifer of the Groningen gas field is experiencing pore pressure decline due to the historical gas production in the Groningen field. The stress changes determine whether faults can be reactivated, which is assumed here as being indicative for induced seismic slip. In general, we find that the main thermo-elastic stress changes are associated with the cooled volume of the aquifer centered around the injector, reaching up to 1.5 times the cooled-zone radius (i.e. distance from injection well to the edge of the cooled reservoir volume). Poro-elastic effects are less important in the context of the SW aquifer. Reactivation of faults is also mainly concentrated in this cooled zone. Therefore it is important to map both the cooled volume and the geometry of faults that may be reactivated and may be seismogenic. The radius of the cooled reservoir volume depends on the volume of injected cold water, the height of the permeable zone and the thermal properties of the fluid and the rock. We suggest methods to monitor the cooled reservoir zone, including well testing, pulse testing and DTS. Non-depleted parts of the aquifer are typically slightly more stable, less prone to fault reactivation, and hence less seismogenic. However, this does depend on the geomechanical parameters chosen (specifically on the Poisson's ratio and Biot constant).

Finally, it is important to assess the offset of a fault when it is present in the cooled or depressurized zone of a geothermal field. An offset equal to the aquifer thickness, with the top of the hanging wall at the same depth as the bottom of the footwall, maximizes the effect of depletion and cooling on the induced stresses. This is the case for the complete range of values for the dip of the fault.

In general, uncertainties in input parameters are important to consider and should be taken into account in any project-specific analysis of geothermal operations. A number of key inputs is identified in this study: virgin in-situ stress state, fault frictional properties, elastic moduli.

The work described here has focused on generic results that are broadly applicable to all potential geothermal projects and is no direct input for a particular operation. However, due to their broad applicability, the results from this project can serve as important input to studies targeted at such operations.

Contents

Contents

1 Introduction

This report is part of the KEM-19b project, which focusses on the behavior of the southwest (SW) aquifer of the Groningen gas field. In report KEM-19b Part-1 (TNO 2025 R10452) we have reported on the geological modelling, reservoir flow modelling, seismicity analysis and seismic hazard assessment. The main focus of that work is on the long-term pore pressure evolution of the aquifer, and the corresponding effects on seismicity and seismic hazard.

The final research question of the KEM19b project focusses on the potential use of the SW aquifer of the Groningen gas field as a source for geothermal energy. In particular, this part of the study aimed to address the following research questions:

1. What areas are more prone or less prone to induced seismicity due to possible geothermal exploitation?
2. To what extend would a possible future geothermal exploitation of the aquifer impact the seismic potential of the aquifer? At what distance from a possible geothermal operation is the magnitude of stress change negligible?

The first question is addressed in Chapter 2 of this report, where we look at the SW aquifer's tendency to respond seismically to stress changes, utilizing the Groningen seismic source model framework. We call this tendency for seismicity the *seismicity propensity*. In particular, we focus on how the *seismicity propensity* varies spatially. This investigation therefore allows us to draw conclusions on which parts of the SW aquifer are expected to respond more/less seismically to geothermal operations, without having to make assumptions about the operational parameters of the geothermal project.

The second question in fact contains a number of sub-questions:

a. What is the expected magnitude of the stress changes associated with a geothermal project?
b. What is the spatial extent of these stress changes?
c. How are they impacted by the fact that the SW aquifer's pore pressure is declining over time due to the past gas extraction of the Groningen gas field?

These questions are addresses in Chapter 3, where we employ two semi-analytical tools (PANTHER and SRIMA) to investigate the stress changes around a geothermal project, under a range of different geomechanical parameters. Fault reactivation as a result of stress changes is taken as indicative for the induced seismicity potential.

2 Seismicity propensity

2.1 Introduction and approach

One of the main research questions for this project is 'What areas in the SW aquifer are more prone or less prone to induced seismicity due to possible geothermal exploitation?' Although the extent and magnitude of stress changes due to geothermal operations will critically depend on the specifics of the project, we can still identify areas that are more sensitive to stress changes without making reference to any specific project, or any specific operational parameters. We do this by applying a uniform forcing (a pore pressure change of a given amount), and calculate induced seismicity rates based on this, utilizing the Groningen seismic source model framework which relates reservoir compaction to seismicity rates. This will result in a map with an expected event rate for an identical amount of 'external forcing' at all locations in the SW aquifer. Such a continuous map indicates which areas are more and less prone to induced seismicity in general, and therefore also to induced seismicity due to a geothermal project. Although we apply a uniform pore pressure change (rather than a uniform temperature change), within the context of the Groningen seismic source model these quantities are actually interchangeable. This can be shown by considering the proposed update to the seismic source model for Groningen which includes temperature effects (TNO, 2024b). The derivations in that report show that the original Groningen seismic source model, in which vertical strain at offset faults generates seismicity, can be extended by including the temperature-dependent strain in the vertical strain term:

$$\varepsilon_v = -\frac{1}{H}\alpha\Delta P_p - \frac{(\nu+1)}{(1-\nu)}\alpha_T\Delta T \tag{1}$$

where ε_v is the vertical strain, H is the uniaxial elastic modulus, α is Biot's coefficient, ν is Poisson's ratio, α_T is the thermal expansion coefficient, ΔP_p is the pore pressure change (depletion defined as negative), ΔT is the temperature change (cooling defined as negative).

To show that an arbitrary pressure change is in fact interchangeable with an equivalent temperature change we define a new model parameter a_T^* (purely for convenience):

$$a_T^* = H\alpha_T \tag{2}$$

Substitution of (2) into (1) gives:

$$\varepsilon_v = -\frac{1}{H}\alpha\Delta P_p - \frac{(\nu+1)}{(1-\nu)}\frac{a_T^*}{H}\Delta T \tag{3}$$

We can then (again for convenience) define $a_T = a_T^*\frac{\nu+1}{1-\nu}$ to obtain

$$\varepsilon_v = -\frac{1}{H}\alpha\Delta P_p - \frac{1}{H}a_T\Delta T \tag{4}$$

And finally:

$$\varepsilon_v = -\frac{1}{H}(\alpha\Delta P_p + a_T\Delta T) \tag{5}$$

This shows that, for the purposes of calculating vertical strain ε_v, an arbitrary change in temperature without changing the pore pressure ($\Delta T = C, \Delta P = 0$, where C is an arbitrary value for ΔT), can be replaced with an equivalent change in pressure without changing the temperature ($\Delta P = \frac{\alpha_T}{\alpha} C, \Delta T = 0$). In the context of the Groningen seismic source model (Bourne and Oates, 2017), ε_v at offset faults (through Coulomb stress change ΔC) is the driver for seismicity. In this model, a given amount of vertical strain leads to the same stress change ΔC, regardless of whether the vertical strain is caused by a pore pressure change or temperature change. This is due to the 'amplification' of stresses at offset faults (see Bourne and Oates 2017 for details) in the simplified 'thin-sheet' geometry.

By applying this approach of equivalent pressure and temperature change, we are implicitly assuming that the assumptions behind the Groningen seismic source model, which was developed for dealing with pressure changes, remain valid in the context of temperature changes. Specifically, we assume that the induced strains are primarily uniaxial in nature, which is a sensible assumption in the context of pore pressure-induced strains in a laterally extensive, highly permeable reservoir, remains true for geothermal operations.
We acknowledge that strains induced by typical geothermal operations are less uniaxial in nature, due to their relatively large spatial temperature gradients. However, we believe that for a first-order assessment of seismicity propensity, the chosen approach is sensible and valid. After all, we are investigation *seismicity propensity* which can be seen as an expression of the probability of encountering faults that are near failure and only need a small stress disturbance for failure to occur. In the case of the SW aquifer of the Groningen field, to what extent faults are near failure is determined by their stress history, which is determined by pressure depletion. In other words, although the uniaxial strain assumption may not be fully valid for modelling the stress disturbance caused by geothermal operations, it is a valid assumption to describe the stress history of the faults, and therefore of their propensity for failure and seismicity.

2.2 Results

Here we choose to apply a spatially uniform 1 MPa pressure depletion (approximately equivalent to a 5 °C cooling for typical parameter choices), to identify where in the SW aquifers the combination of reservoir stiffness (H), pressure depletion, and fault geometry is most prone to the generation of induced seismicity. The magnitude of the depletion (1 MPa) is arbitrary in some sense, since we're interested in evaluating how different parts of the reservoir respond to *the same* forcing. We here choose an equivalent forcing that is expected to be reached by any geothermal project (5°C cooling) to investigate the spatial differences in seismicity propensity. Since the relation between vertical strain and the rate of induced seismicity is exponential, it is possible that this spatial picture changes when the reservoir pressures evolve though time. We therefore apply the 1 MPa depletion at two points in time, once in 2025, and once in 2053 (the final year of the pore pressure simulations). To account for the uncertainty in pore pressures and reservoir compressibility, we apply this depletion to all 66 vertical strain ensemble members and show the mean ensemble result. The calibration of the source model is performed on each ensemble member individually. For details, see the other report on KEM19-b (TNO, 2024a).
The seismic source model contains a spatial smoothing step, which smooths the incremental Coulomb stress changes on faults, before calculating the seismicity rate. This means that each fault segment influences the seismicity rate in the surrounding area (several kilometers in practice). This has two consequences that are undesirable from the perspective of the

research question at hand. First, it means that even though the loading (pressure change) is only applied in the aquifer, the stresses reach into the Groningen gas field. Because of the past depletion in the reservoir, and the exponential relation between stress changes and seismicity, this means that the loading in the aquifer mostly affects the seismicity within the Groningen gas field. The second consequence is that the seismicity rate forecast resulting from a uniform pressure depletion is spatially rather smooth. However, for this particular research question, we are interested in finding the fault locations that are particularly prone to seismicity. For these reasons, the spatial smoothing of incremental Coulomb stress changes is omitted in the forecasting. This results in more specific field locations which 'light up' as being prone to the generation of seismicity upon stress changes due to their stress history, compressibility, fault throw and fault density. For visualization purposes, we do apply a smoothing kernel with a small standard deviation (500m, 1 pixel) to the resulting seismicity rates to obtain a continuous seismicity propensity map (Figure 1). In addition, in Figure 2 a map with a different color scale is shown to provide a more detailed view of the seismicity propensity map for parts of the SW aquifer that are difficult to see in Figure 1.

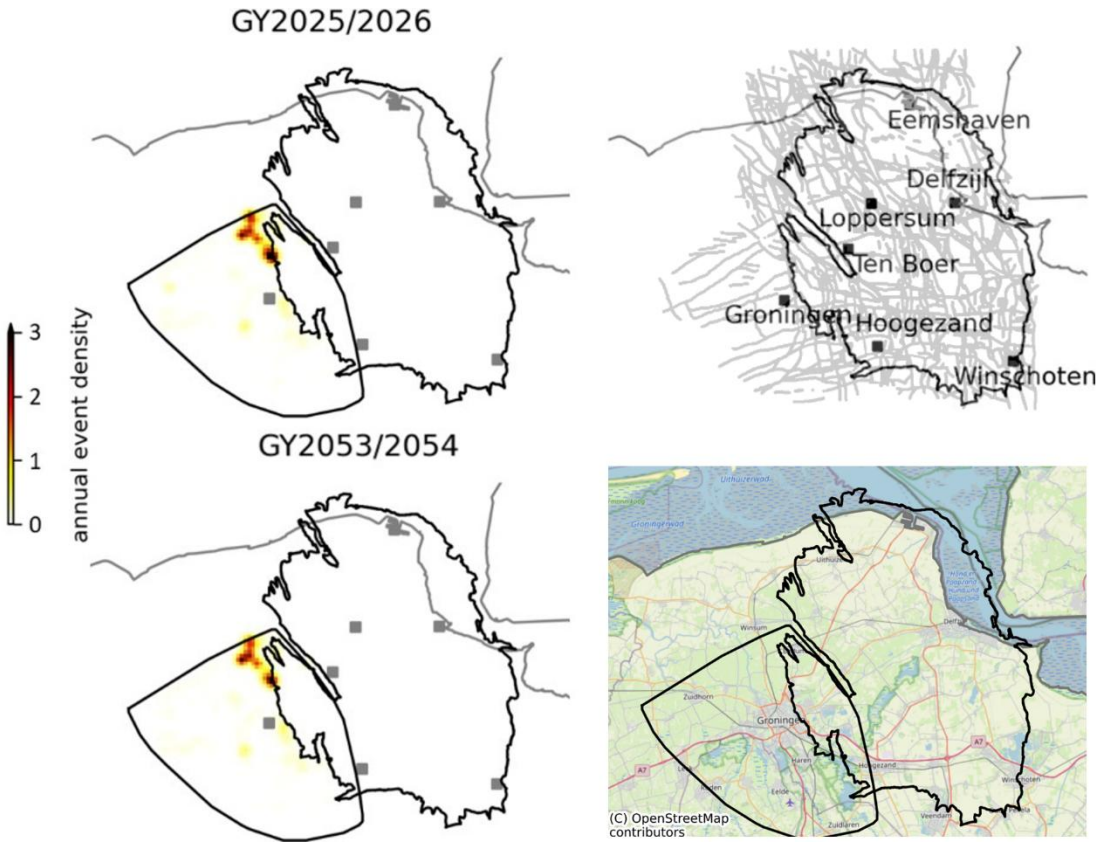

Figure 1: Relative seismicity propensity (arbitrary scale). Generated by applying a 1MPa pressure depletion throughout the entire SW aquifer for gas year 2025/2026 and 2053/2054. Model is calibration is identical to that described in Chapter 4 of the KEM19b report (Part I). The pressures outside the SW aquifer are kept constant and faults within the Groningen field are not considered in the seismicity calculation.

The resulting maps show that the seismicity propensity of the SW aquifer does not vary significantly with time. Given the same loading, the area just north of the city of Groningen is expected to be the most prone to seismic activity. This is largely explained by the high pressure depletion in this area (Bedum field), leading to comparatively high Coulomb stress development compared to other areas in the SW aquifer. Due to the exponential relation between Coulomb stress and seismicity rate, a similar amount of loading has a larger effect on seismicity in this area.

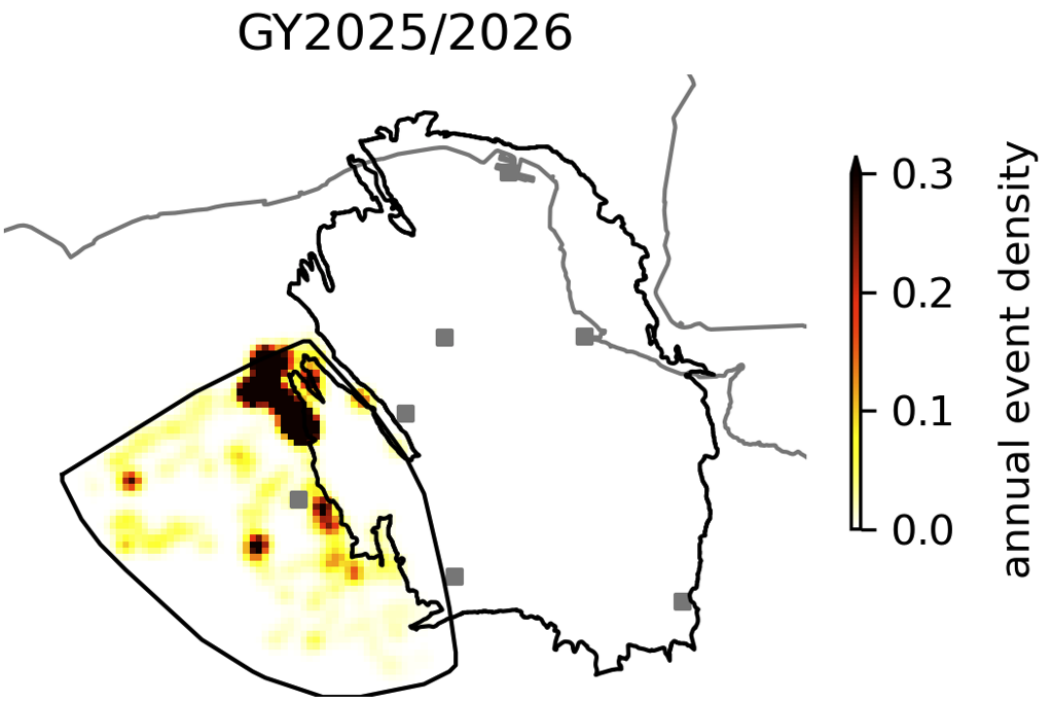

Figure 2: As Figure 1, but with the color scale maximized at 10% of the full scale. This allows for more detail to be shown in areas more to the southwest. It is important to note that due to the 'clipping' of the color scale, areas that appear black may represent different values (i.e. the seismicity propensity around Bedum is still significantly higher than the seismicity propensity in the east and southwest of the city of Groningen, despite both showing the same color on this map). This figure is meant to show relative differences in the SW aquifer that are difficult to see in Figure 1, due to the impact of the area around Bedum.

3 Extent and magnitude of the stress impact of geothermal operations

3.1 Introduction

The areal extent, temperature and permeability of the SW aquifer make it a potential target area for geothermal energy. A pressing question is how geothermal operations would change the probability of induced seismicity of the area. We have seen (TNO 2025 R10452) that the depletion of the aquifer due to equilibration with the surrounding gas fields causes a change in the probability of induced seismicity. Geothermal energy operations introduce more pressure changes since water will be injected (local pressure increase) and produced (local pressure decrease). In addition, temperature changes around the injection wells will occur as the reinjected fluids are usually 10's of degrees cooler than the initial reservoir temperature. Both pressure and temperature changes impact the total and effective stresses. These stress changes change the potential for fault reactivation, and, assuming fault reactivation results in seismic fault slip, will consequently change the seismic potential of the area. We here report on an initial assessment of the magnitude of the stress changes and fault reactivation.

As a first step we wish to investigate to what extent a possible future geothermal exploitation would impact the probability of induced seismicity by making a first-order assessment of both its area of influence and its magnitude of influence.

In order to assess the influence of a geothermal project on seismicity, the ideal approach would be to incorporate the ensuing stress changes into the model determined above. However, due to the large number of operational variables involved (production/injection rates, re-injection temperature, doublet configuration and location), this is infeasible to do in a generic non-project specific sense. In addition, the seismicity proxy 'smoothed incremental Coulomb stress' is difficult to interpret as a 'physical' quantity. This makes it difficult to superpose any stress changes derived outside of the Groningen source model framework to the Groningen source model. Also, the effective stress changes resulting from a geothermal project in a sandstone reservoir as the Slochteren Sandstone Member are fundamentally different from those resulting from depletion. First of all, even though in both cases stress changes can be destabilizing, for cooling the effective stresses become less compressive, and for depletion the effective stresses become more compressive. Second, the space-time behavior is different because thermo-elastic stress changes develop in a cooling rock volume progressively growing in size, whereas poro-elastic stress changes from depletion occur gradually over the entire reservoir as the pressure changes (Buijze et al. (2023); Mathur et al. (2024)). Still, the initial state of stress or initial fault criticality and the fault characteristics are crucial input in both cases.

We therefore have chosen to assess the impact of a 'typical' geothermal project in the Groningen SW aquifer, starting from the situation where the aquifer has been depleted with regard to the virgin pressures. We use the semi-analytic mechanical models SRIMA (Seal and Reservoir Integrity Mechanical Analysis, developed at TNO, Buijze et al. (2022), https://www.nlog.nl/sdra-geothermie-integriteit-afdichtend-pakket) and PANTHER v0.7

(Buijze et al. (2022), https://github.com/TNO/PANTHER). SRIMA models both pressure and temperature effects on the stresses for a radially symmetric case. PANTHER models pressure and temperature effects on the stresses on a fault in a vertical plane-strain situation in which a reservoir crosses a dipping fault with an offset between the two sides.

3.2 Definition of the base cases

The starting situation of the geothermal base cases is the depleted SW aquifer. For the reservoir characteristics (depth, thickness, permeability, porosity) we take values given earlier (TNO 2024a).
Important properties are the elastic parameters. For the virgin in-situ stresses we take values from Bakx et al. (2022). We take a value of 22.6 MPa/km for the gradient of the lithostatic vertical stress; 17.8 MPa/km for the gradient of the minimum in-situ stress in the target sand layers and 18.3 MPa/km in the overlying and underlying, more claystone-rich layers. Elastic moduli have been shown to vary considerably with porosity, and sandstones from the Groningen gas field have even been shown to behave partly inelastic (Pijnenburg et al. (2018)). We use a base case value of 14 GPa but account for a range of 7 – 20 GPa. For Poisson's ratio we take a value of $\nu = 0.15$. Heat flow properties (heat capacity; thermal conductivity) are given representative numbers. Parameter values are presented in Table 1.

For the connection with induced seismicity, we evaluate the induced stresses in terms of change of the Coulomb Failure Function (ΔCFF) and Shear Capacity Utilization (SCU) on a fault. The two measures are defined as:

$$\Delta CFF = \Delta\tau - f_s \Delta\sigma_n'$$
$$SCU = \left| \frac{\tau}{C + f_s \sigma_n'} \right| \quad (6)$$

in which τ is the shear stress, C the cohesion, f_s the friction coefficient and σ_n' the effective normal stress. ΔCFF signifies how the stress changes with respect to the Mohr-Coulomb failure envelope, with positive values indicating the stress gets closer to failure, and negative values indicating the stress becomes more stable. The SCU measures the ratio of the shear stress with respect to the failure stress, with 1 as the critical value at which the shear stress equals the fault shear strength and reactivation occurs. We also define a typical fault geometry at critical orientation close to the injection well (150 m distance), but not intersected by it.
One of the most important input parameters that are analyzed are the starting values for the in-situ stresses, which are different from the virgin in-situ stresses because of the depletion of the aquifer. This depletion varies over the aquifer area spanning a range of 0 – 20 MPa. However, the distribution is relatively smooth, and we make the approximation of uniaxial compaction in order to calculate the starting stresses when starting a geothermal operation in a depleted area. Such compaction involves a constant total vertical stress and a decrease of the total horizontal stresses with a stress path coefficient (ratio of total horizontal stress change with respect to pressure change):

$$\gamma_h = \frac{\Delta\sigma_h}{\Delta P} = \alpha_p \frac{1 - 2\nu}{1 - \nu} \quad (7)$$

Typical Mohr diagrams for uniaxial compaction are drawn in Figure 3 for the starting pressure equal to the virgin pressure, and for values of the depletion of 5, 10, 15 and 20 MPa and a friction coefficient of 0.55. The rather small values of Poisson's ratio in combination with a large value of 1.0 for the Biot constant result in a value of γ_h=0.824 and a movement of the

Mohr circle towards the failure line upon depletion (Figure 3a). For a larger value of Poisson's ratio or a smaller Biot constant, depletion can result in movement away from failure. Figure 3b. The uniaxial compaction due to cooling moves towards the failure line much more dramatically (the arrows) than the movement due to the depletion (from blue to red circles).
We consider a typical geothermal doublet where hot water is produced and cold water is injected. We only assess the stresses around the injector since here the destabilization is largest due to increased pressures and decreased temperatures. For the thickness and permeability of the SW aquifer, we consider an average injection rate of 300 m^3/hr at an injection temperature of 35°C.
An important parameter in the assessments following is the size of the cooled zone. The upper limit of the radius of the cooled zone, which is the value when there is no leakage of heat to the seal and the base, is given by (Buijze et al, 2022).

$$r_{cooled}^{max} = \sqrt{\frac{V_{inj}}{H\pi} \cdot \frac{\rho_w c_w}{\rho_r c_r}} \tag{8}$$

Here, $V_{inj} = Q_{inj} \cdot t$ in the volume of injected fluid; H the height of the aquifer zone; ρ_w and ρ_r are the densities of the injected fluid and of the gross rock; and c_w and c_r are their respective heat capacities. In most of the cases this value can serve as a good estimate.

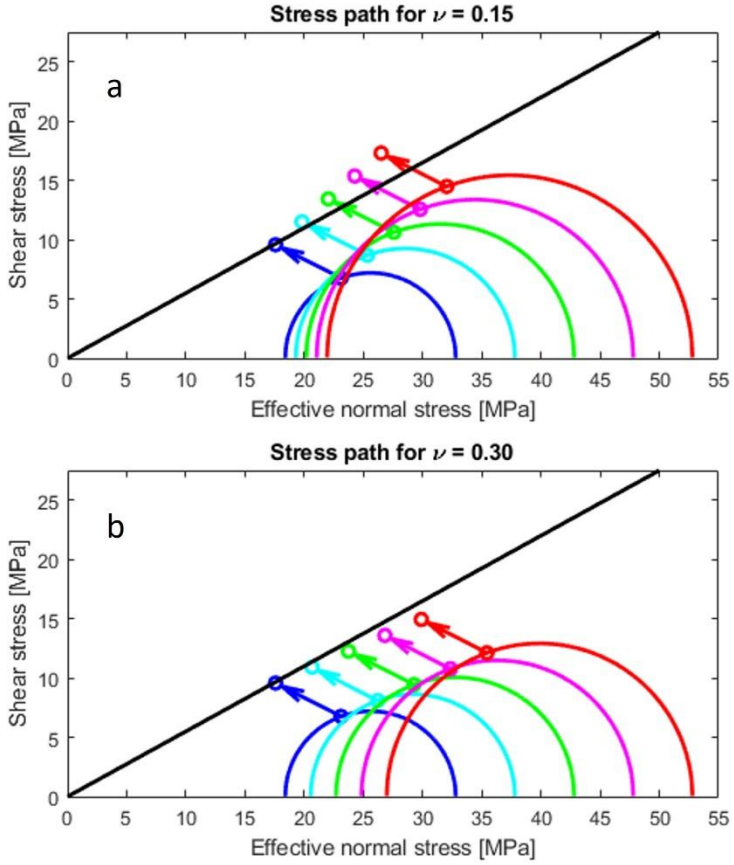

Figure 3 Typical stress path during uniaxial depletion and subsequent cooling. Mohr circles represent tractions on planes with different orientation. The depletion is 0, 5, 10, 15, 20 MPa for the blue, cyan, green, magenta and red circles. Geothermal injection is assumed to yield 0.5 MPa pressure increase, 7 MPa decrease of the principal horizontal stress and 1 MPa decrease of the principal vertical stress. Top and bottom figures represent Poisson ratios of 0.15 and 0.30, respectively.

3.3 SRIMA

3.3.1 The Tool

The assessment of potential seismicity requires the calculation of induced changes of pressures, temperatures, associated stress changes, the potential reactivation of faults, estimate of a maximum magnitude and the propagation of seismic waves to the surface. Due to large uncertainties in the input and the inherent irregular behaviour of seismicity, such calculations should ideally be performed stochastically. The tool SRIMA (acronym for Seal and Reservoir Integrity Mechanical Analysis) has been designed and developed for this purpose. It is a tool that calculates the above for radially symmetric geometries with injection in a reservoir layer that is sandwiched between a seal and a base layer. In the current study we have used it as a tool to test sensitivity of pressures, temperatures, induced stresses and reactivation potential to the input parameters.
The radial symmetry of SRIMA (Figure 4) deploys three layers. Advection of heat and a steady-state pressure solution is modelled in the reservoir. In the overlying and underlying layers, vertical diffusion of heat and pressure are modelled according to diffusivity laws in drained rock. Stresses are calculated for these geometries based on linear poro-thermo-elasticity, to be combined with the starting stresses in order to arrive at total and effective stress fields. From those, the increase in Coulomb Failure Function, ΔCFF, and the Shear Capacity Utilization SCU are calculated (Eq. 6). The calculations can be performed either in points on a line (for faults potentially present at those points at most critical orientation) or on a pre-defined fault plane. We limit the SRIMA evaluation to these outcomes; the connection to seismicity will be made outside SRIMA in the next Section of this report. For a more extensive description of SRIMA we refer to Buijze et al. (2022); Fokker, et al. (2023); Fokker & Wassing (2019).

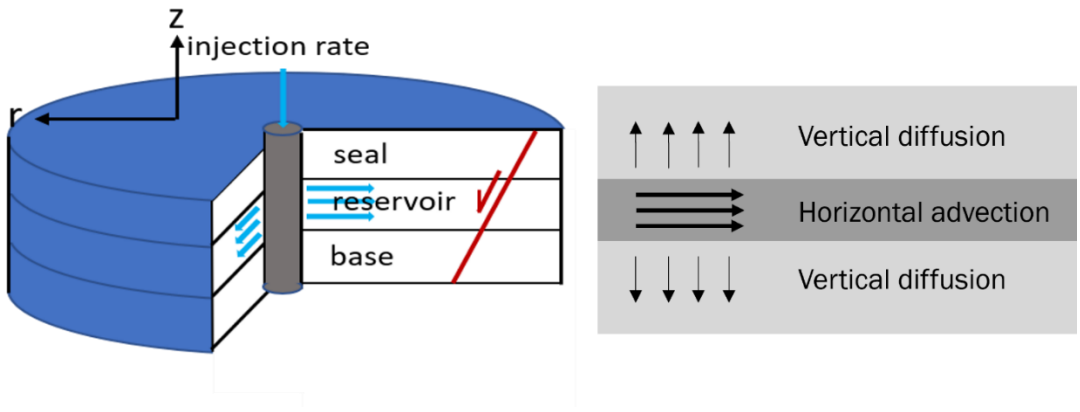

Figure 4 SRIMA geometry: Radially symmetric with injection over entire reservoir interval. Darcy flow and advection in the reservoir layer; diffusion above and below.

3.3.2 The model cases

SRIMA results were output at three different geometries: on a vertical line at the edge of the injection well; on a horizontal line starting from the wellbore into the aquifer in the middle of the reservoir; and on the pre-defined fault at 150 m distance from the well. For the vertical and horizontal lines, stochastic calculations were performed as well, to assess the influence of various uncertain parameters on measures that connect to induced seismicity.
The base case model outcomes involve calculations with five values of the starting aquifer pressure: 35 MPa (virgin pressure), 30, 25, 20 and 15 MPa, with corresponding initial horizontal stresses in the reservoir calculated through Eq. 7, assuming no initial pressure diffusion into

seal and base. These values have been chosen to represent the pore pressures at different positions in the SW aquifer. The values of the input parameters are reproduced in Table 1. The values for the virgin aquifer and the values after depletion represent the base cases; the value ranges for stochastic calculations have been used for Monte Carlo drawings of those parameters. Note further that the stress contrasts are chosen to reduce the stress in the aquifer layer, and that fault strike is not in the table since there is no horizontal stress anisotropy.

Table 1 SRIMA input parameters: Base Case values for virgin and for depleted aquifer; and ranges used.

Input parameter	Values for Virgin Aquifer	Values after depletion	Values for Stochastic calculations
Top depth	3000 m		3000 m
Thickness	300 m		150 – 400 m
N/G	70%		70%
Fault Dip	60°		
Reservoir temperature	100°C		100°C
Reservoir pressure at top	35 MPa	30 / 25 / 20 / 15 MPa	25 MPa
Pressure Contrast Seal To Reservoir	0 MPa	-5 / -10 / -15 / -20 MPa	-10 MPa
Pressure contrast Reservoir to Basement	0 MPa	5 / 10 / 15 / 20 MPa	10 MPa
Salinity	200,000 ppm		200,000 ppm
Permeability	100 md		50 – 500 md
Porosity	20%		20%
Heat capacity (saturated rock)	850 J/kg.K		850 J/kg.K
Thermal conductivity (saturated rock)	1.1 W/m.K		1.0 – 5.0 W/m.K
Minimum horizontal stress at top reservoir	53.4 MPa	49.28 / 45.16 / 41.05 / 36.93 MPa	42 – 48 MPa
Stress contrast Seal to Reservoir	-1.5 MPa	-4.12 / -8.24 / -12.35 / -16.47 MPa	-8 MPa
Stress contrast Reservoir to Basement	1.5 MPa	4.12 / 8.24 / 12.35 / 16.47 MPa	8 MPa
Vertical stress at top reservoir	67.8 MPa		67.8 MPa
Maximum / minimum horizontal stress ratio	1.0		1.0
Max hor. stress azimuth	135°		135°
Young's modulus	14 GPa		7 – 20 GPa
Poisson ratio	0.15		0.05 – 0.35
Biot constant	1.0		1.0
Linear thermal expansion coefficient (saturated rock)	1.0 10^{-5} K^{-1}		1.0 10^{-5} K^{-1}
MC friction coefficient	0.55		0.5 – 0.7
Cohesion	0 MPa		0 – 4 MPa
Residual friction	0.45		

Injection rate	300 m³/hr		300 m³/hr
Injection temperature	35 °C		20 – 50 °C
Injection duration	25 yr		25 yr

3.3.3 Stress changes with depth

With the low value of Poisson's ratio ($\nu = 0.15$), Biot constant equal to 1 and a friction coefficient of 0.55, depletion results in a stress moving closer to failure (see also Figure 3). The pressure and stress profiles for three of these cases (0, 10, and 20 MPa depletion prior to geothermal injection), along a vertical line close to the injection well, are represented in Figure 5, for the moment of starting cold-water injection and after 1, 5, and 25 years of injection. The pressure changes in the seal and the base are due to the minimum allowable value for the permeability and the assumption of drained conditions. After one year of injection and later, the SCU in the aquifer at the location of the well exceeds unity at the upper and lower aquifer boundaries; the effect is stronger for lower starting pressures (more prior depletion). SCU in the seal and the base quickly diminish with distance to the interface with the aquifer.

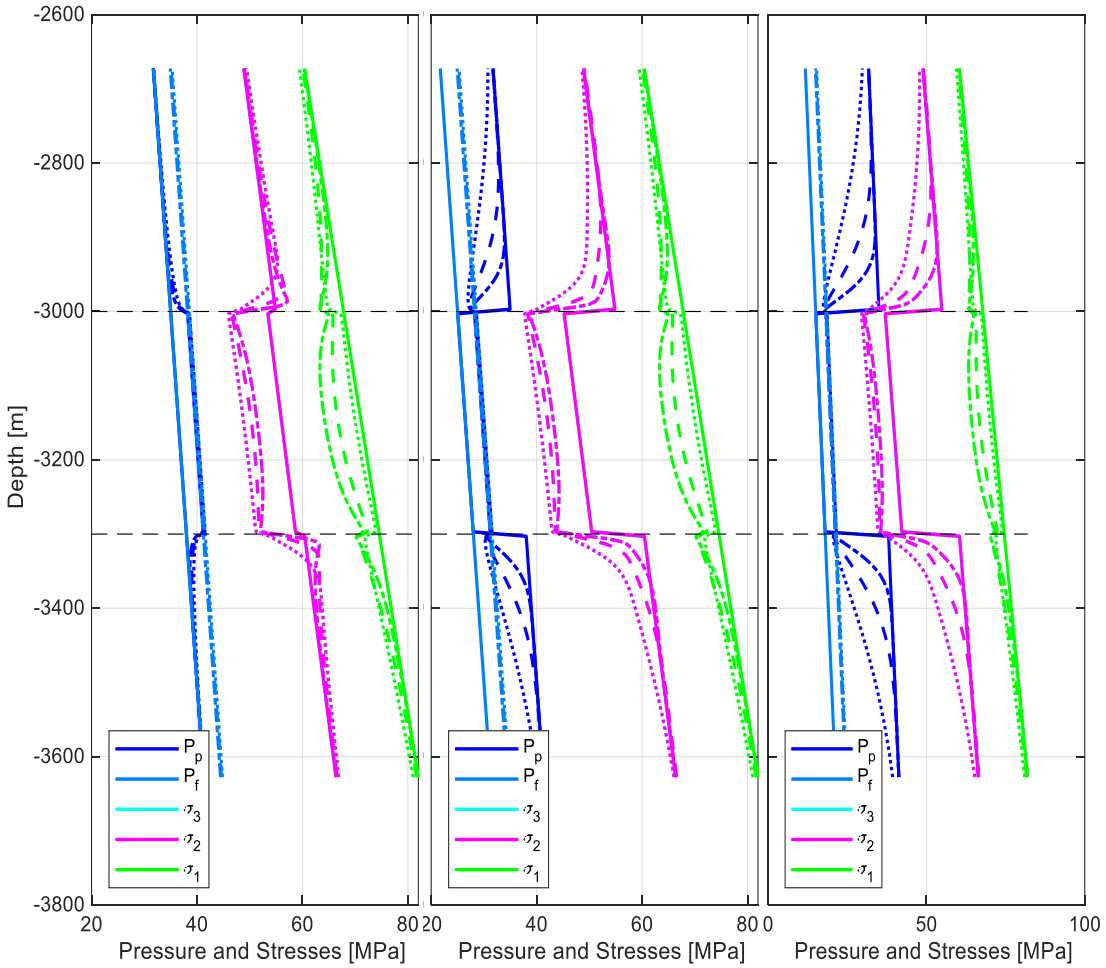

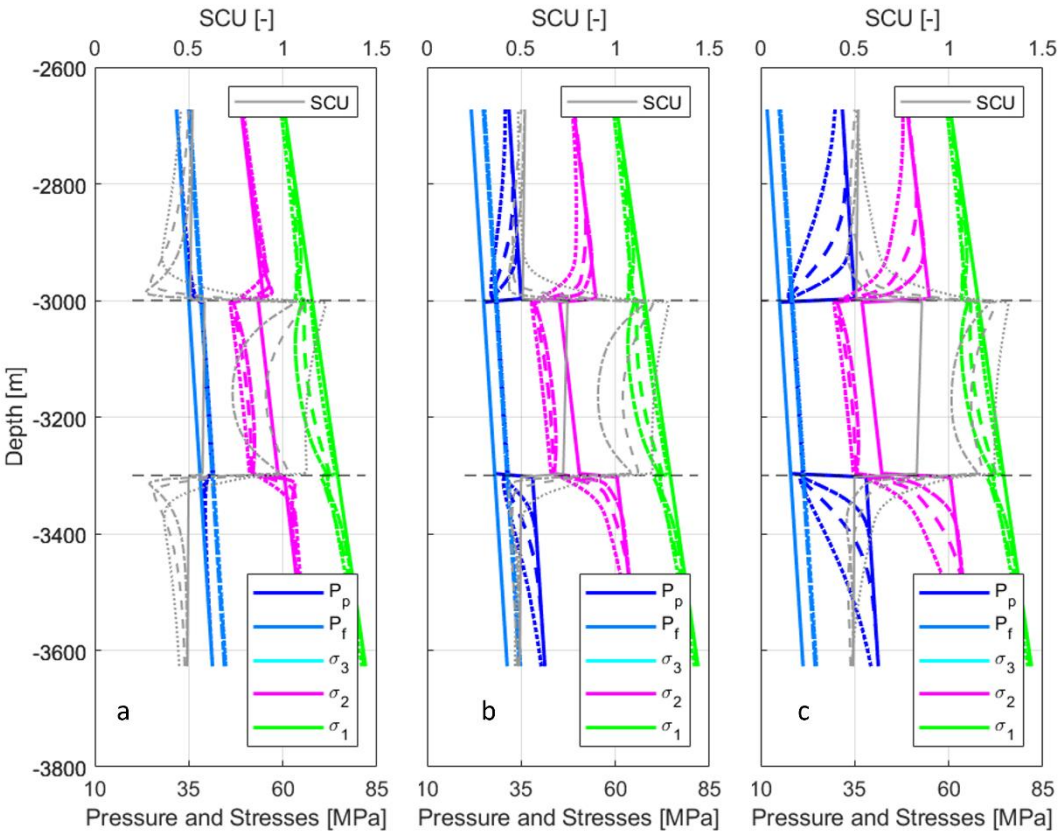

Figure 5 Pressure and stress profiles, and associated SCU along a vertical line close to the injection well. Starting pressure in the aquifer is 35, 25, and 15 MPa (a, b, c). The drawn curves are the starting pressures and stresses; the dashed and dotted ones are the profiles after 1, 5, and 25 years of injection.

3.3.4 Stress changes with distance from the well

An important question concerns the relative contributions of pressure and temperature to the stress changes, for faults at different distances from a geothermal injection well. We want to assess the area of influence and the magnitude of influence of geothermal projects on seismicity. Therefore, we also evaluate the induced stresses and shear capacity on a horizontal line in the aquifer, indicating how they change with distance from the well.

The pressure and temperature *changes* do not depend on the starting pore pressure in the aquifer. Consequently, the starting pressure also has no influence on the induced stress *changes*, including the change in the Coulomb Failure Function. In Figure 6 – Figure 8, the induced changes are presented. A number of observations can already be made from these figures. In the first place, while the cooled-zone radius propagates into the aquifer with injection time, the pressure profile hardly changes (Figure 6). Only a small effect from the larger viscosity of the cooled fluid can be seen because the cooled zone is growing with time. In addition, the pressure changes are concentrated around the wellbore, while the temperature changes reach much further into the aquifer. This has a direct influence on the distribution of the poro-elastic and thermo-elastic stresses. The poro-elastic stresses (right pane in Figure 7) are concentrated around the wellbore; the thermo-elastic stresses (left pane in Figure 7) reach much further into the aquifer, as do the temperature changes. In addition, the difference in shape of the pore pressure perturbation and temperature perturbation make the influence of temperature more important than the influence of the pressure. Clearly, this

balance may shift when input parameters are chosen differently – as an example, the pressure disturbance and the associated poro-elastic stresses are inversely proportional to the permeability and will increase with decreasing permeability.

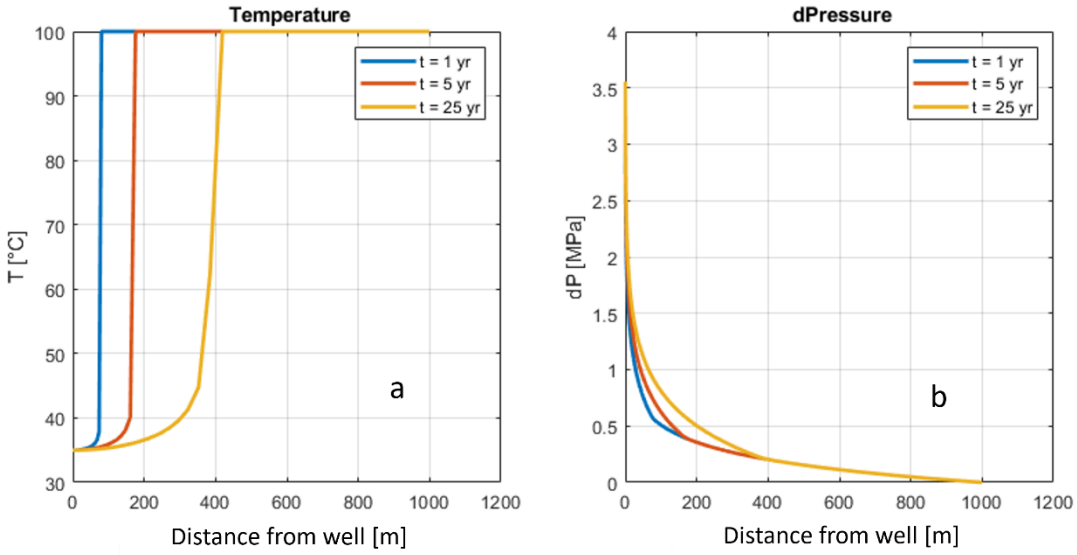

Figure 6 Temperatures (a) and pressure changes (b) in the aquifer. Different colours indicated different times during injection.

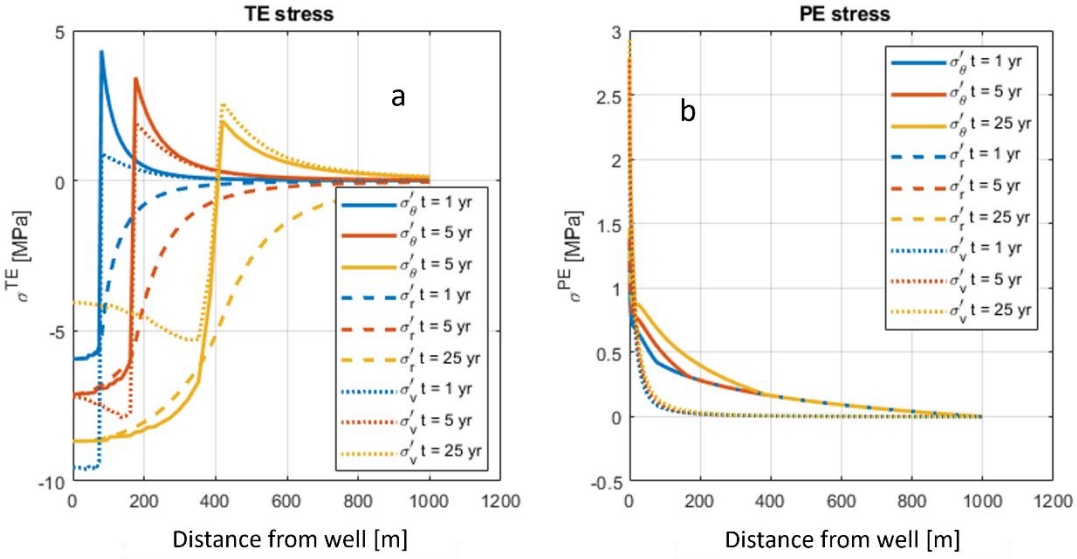

Figure 7 Induced thermo-elastic (a) and poro-elastic (b) stress changes . Colours indicate time since start of injection (1, 5, and 25 years with blue, yellow and red). Line type indicates stress direction (solid curves: tengential; dashed curves: radial; dotted curves: vertical).

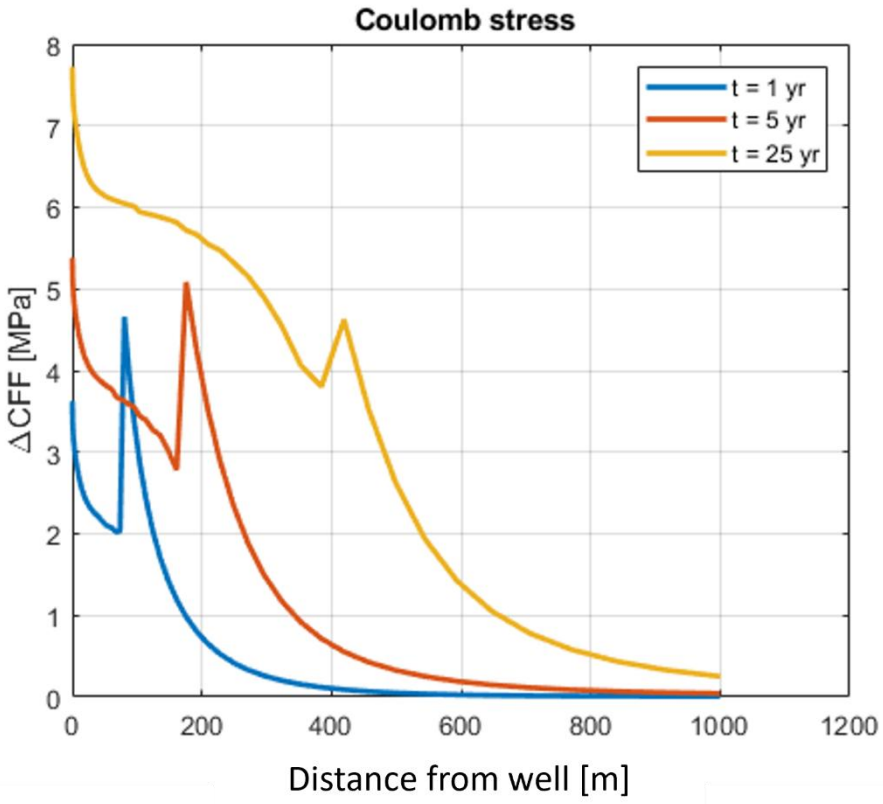

Figure 8 Induced increase in the Coulomb Failure Function as a function of distance to the injection well, for multiple time steps.

An important measure in this analysis is the Coulomb stress. Figure 8 presents the induced changes in the Coulomb Failure Function (ΔCFF, Eq. 6) at a horizontal line in the middle of the aquifer. We see that the *ΔCFF* profile generally follows the cooled zone of the aquifer (cf Figure 6). Close to the wellbore there is an additional effect of the pressure increase that is taking place there. Beyond the cooled zone, ΔCFF diminish to values below 1 MPa at 1.5 – 2 times the radius of the cooled zone. There is a peak in ΔCFF at the cooled-zone radius. This is due to the fast change in temperature with distance at this position, which remains to be present even for longer times, and the associated fast changes in tangential and vertical stresses at the cooled-zone radius. The background of this behavior is the large injection rate, which makes the flow of thermal energy advection-controlled (Nield & Bejan (2006)).
When the induced stress changes are combined with the starting (post-depletion) stress field, the Shear Capacity Utilization (SCU) can be determined. The outcome of this calculation depends on the starting situation. We therefore present in Figure 9 the SCU for aquifer starting depletion of 0, 10, and 20 MPa, for each case after 1, 5, and 25 years of injection. We see that for longer injection times the SCU increases in magnitude and extent. We also see for the larger depletion pressures the starting value of SCU is larger. Regions in the aquifer where more depletion is present at the start of injection show a larger radius for the area where the SCU values are larger than unity. The maximum radii for which SCU is larger than unity are presented in Figure 10.

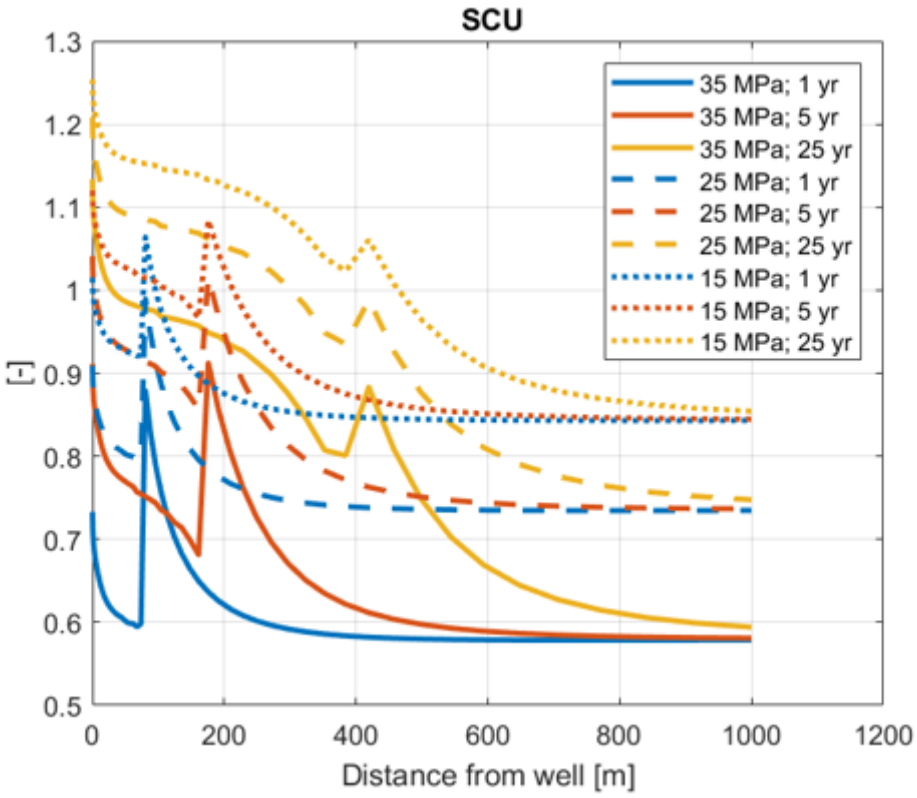

Figure 9 Shear Capacity Utilization (SCU) for the base case calculations after different times of injection (1, 5, 25 years) and for different starting pore pressures (35, 25, 15 MPa) in the aquifer.

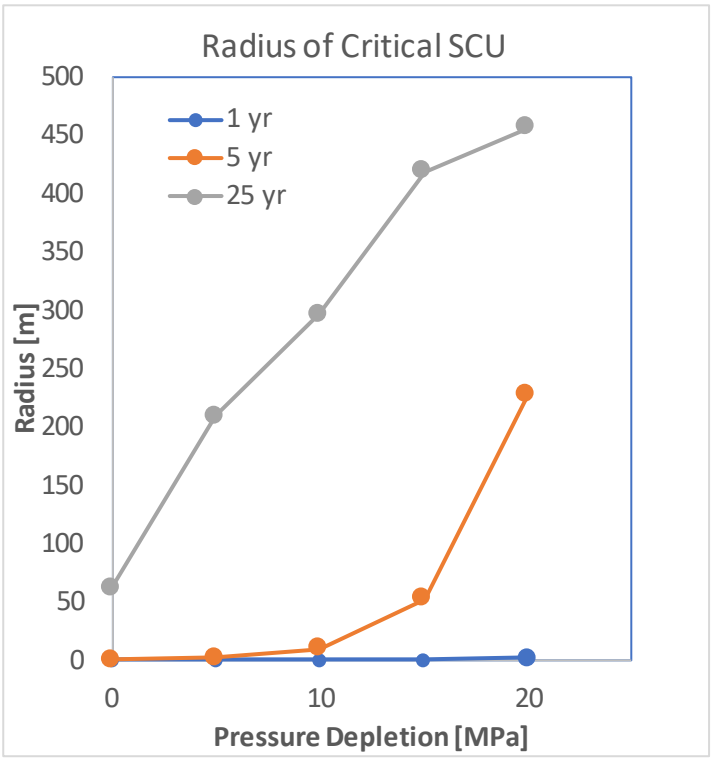

Figure 10 Radius of Critical SCU for different times vs starting depletion of the aquifer.

3.3.5 Stress changes on a predefined fault plane

The modeled fault position at 150 m from the wellbore, along with an indication of the size of the cooled volume, is provided in Figure 11. We give some outputs on the fault for the case starting with 10 MPa depletion. Figure 12 shows how the pressure change and temperature on the fault plane develop. The pressure increase grows with time due to the increased area flooded with low-temperature, high-viscosity water. The cooled zone has not yet reached the fault after one year but a large part of the fault is cooled in subsequent years. While the poro-elastic stress changes are small (maximum 0.7 MPa change of the principal values) and mainly limited to the area near the well, the thermo-elastic stress changes are considerable (Figure 13). They cause the majority of the effect on the stability measures on the fault: the change in ΔCFF and the resulting SCU (Figure 14). The chosen orientation of the fault is near critical; as a result, this is the worst case in the context of fault reactivation. For faults with different orientations, the induced stresses are less critical. The change in ΔCFF does not depend strongly on the dip angle when varying it between 52° and 69°; the SCU decreases substantially when moving away from the critical fault orientation. This is demonstrated in Figure 15 and Figure 16.

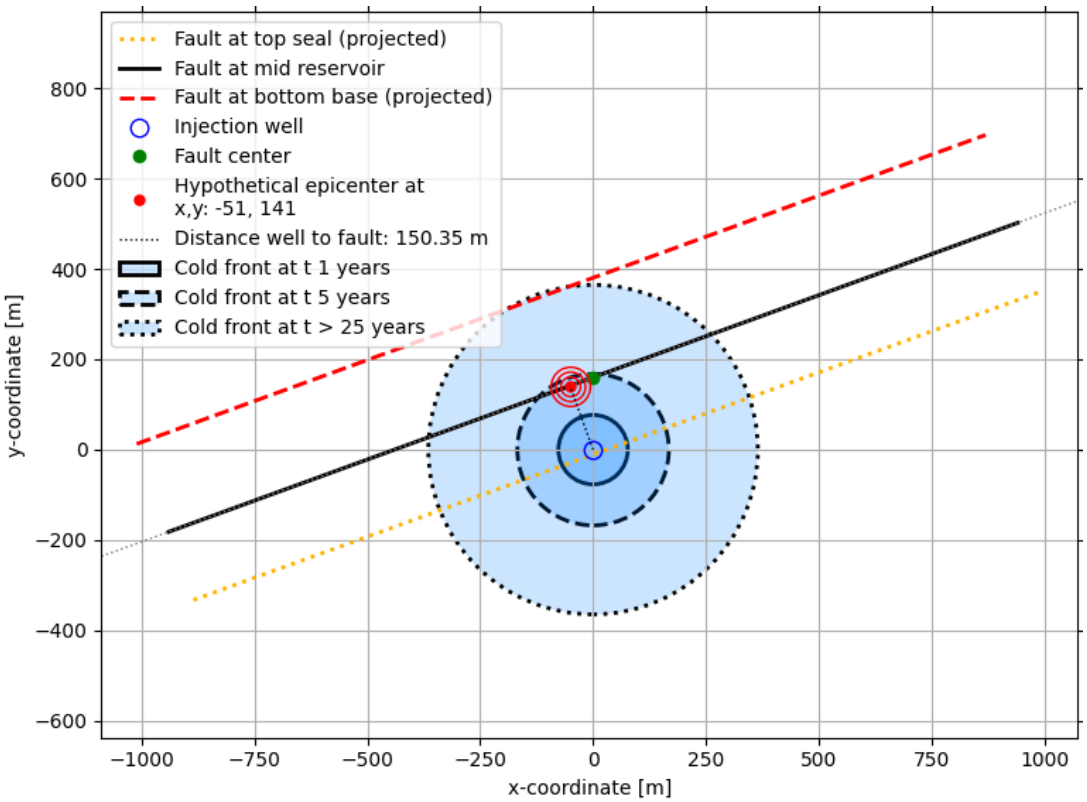

Figure 11 Position of the modelled fault plane with respect tot the injection well and the cooled zone after 1, 5, and 25 years of injection.

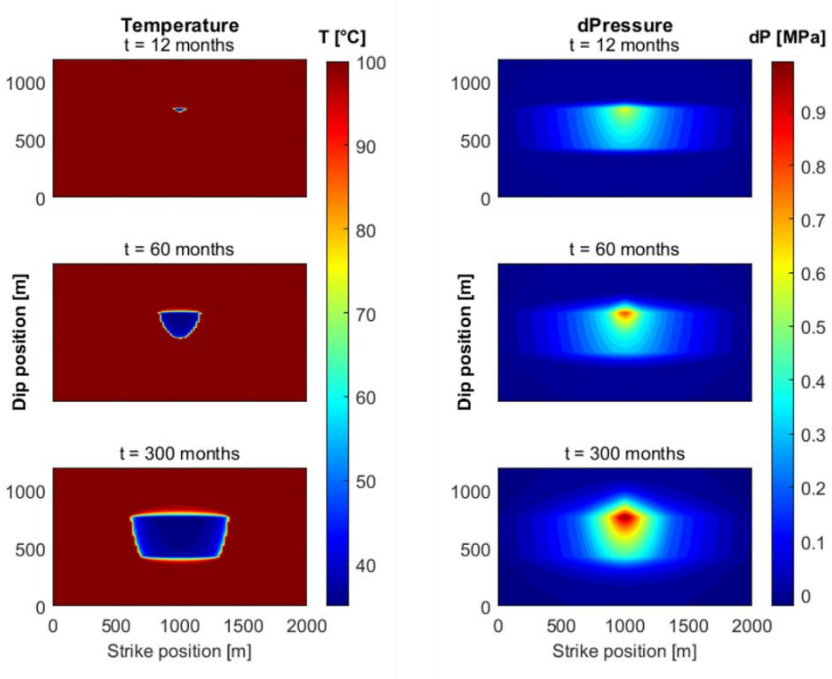

Figure 12 Pressure change and temperatures on the fault.

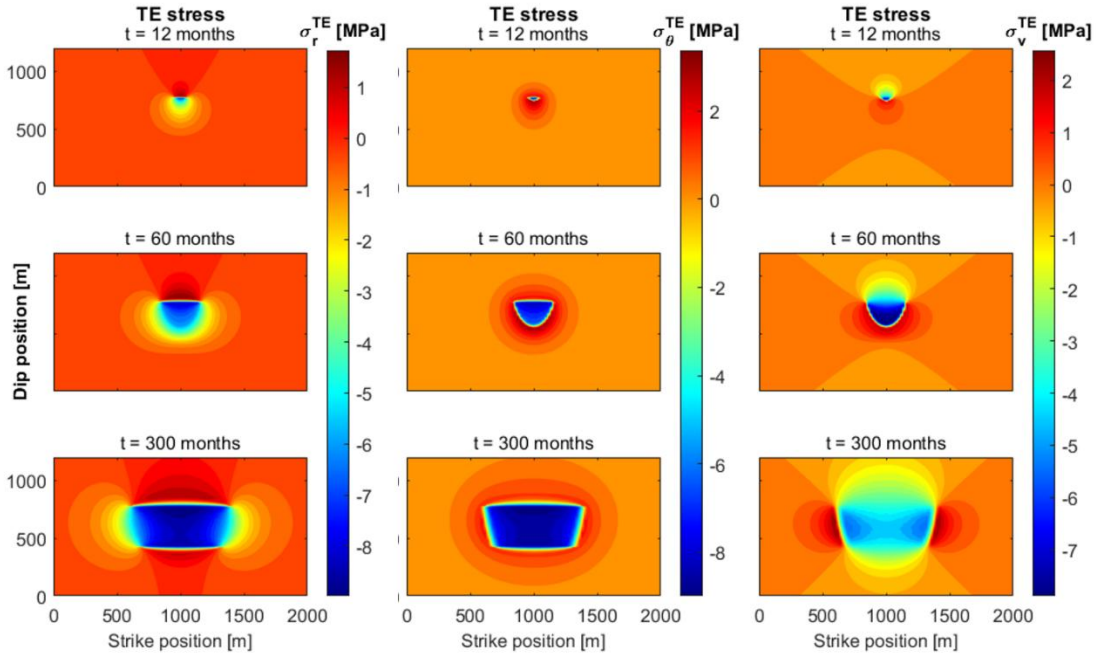

Figure 13 Induced thermoelastic stresses on the fault plane: radial, tangential and vertical stresses for the case with 10 MPa depletion.

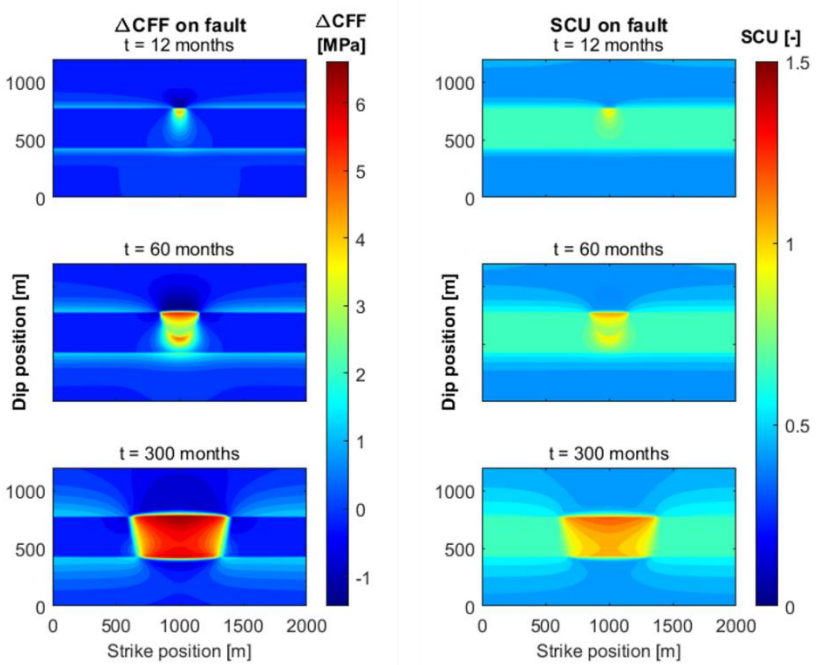

Figure 14 Stress measures on the fault: Change in Coulomb Failure Function (ΔCFF) and Shear Capacity Utilization (SCU) for the 10 MPa depletion case and a fault orientation of 60°.

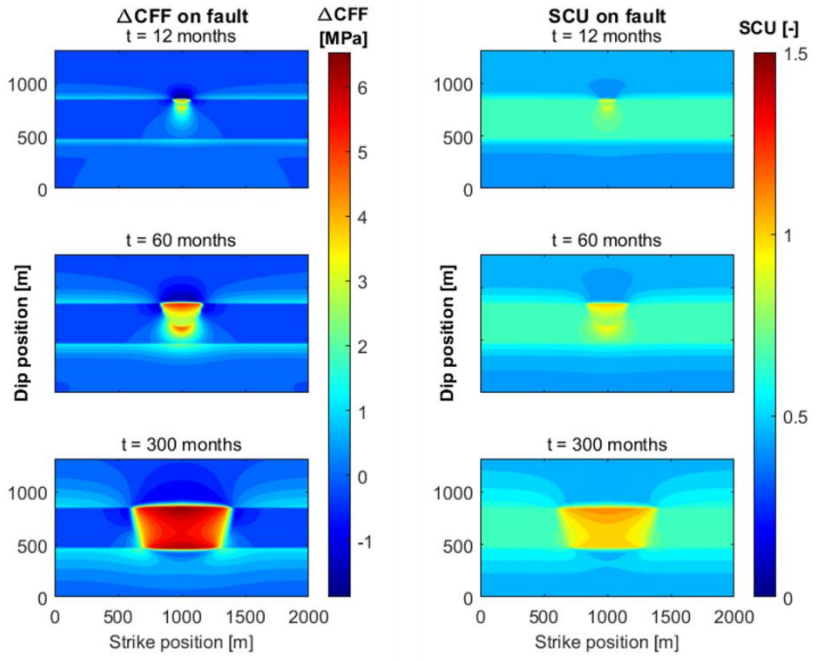

Figure 15 Stress measures on the fault: Change in Coulomb Failure Function (ΔCFF) and Shear Capacity Utilization (SCU) for the 10 MPa depletion case and a fault orientation of 52°.

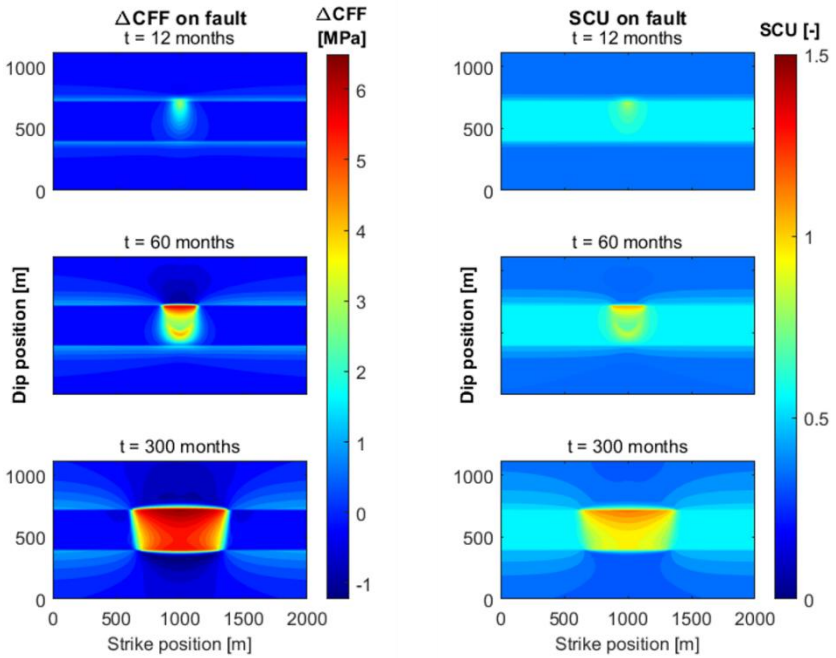

Figure 16 Stress measures on the fault: Change in Coulomb Failure Function (ΔCFF) and Shear Capacity Utilization (SCU) for the 10 MPa depletion case and a fault orientation of 69°.

3.3.6 Stochastic analysis for calculations vs depth

We want to obtain insight in the range of outcomes that are possible with the uncertainty of the input parameters, and to uncover their respective influence. We first performed such analysis on a vertical line, starting from the base case in Section 3.3.3, with a starting value for the aquifer pressure of 25 MPa (10 MPa depletion). The vertical line allows to investigate the effect in overburden and base. For the stochastic analysis, 1000 model values for all uncertain parameters in the last column of Table 1 were drawn randomly within their confidence range.

For the stochastic calculations, a number of measures are present in SRIMA that connect to induced seismicity. The most important for the calculations on a vertical line is the vertical extent to which $SCU > 1$. This is an indication for possible height growth of fault reactivation in the seal. Figure 17 shows the probabilities of reaching certain heights, for all simulations. Less than 10% of all cases show reactivation more than 15 m into the seal, even after 25 years.

Figure 18 shows how the activated cases relate to the driving parameters. In this figure we have ranked the results against the uncertain parameters. First, the propagation of reactivation into the seal has been determined, for each ensemble member. Then, for each input parameter that was varied in the stochastic analysis (e.g. H_{res}, k_{res}) the results were binned in 9 bins, spanning the full range between the minimum and maximum value of the parameter that was explored in the stochastic analysis. Per bin, the normalized fraction of model results for a certain value of the reactivation penetration are indicated with the different colors. The lowest bin represents the cases without reactivation, then we have bins with values smaller than 1.9 m; between 1.9 m and 3.8 m, etc. For instance, within the first E_{seal} bin between 7 and 8.4 GPa, we see no reactivations. For the last E_{seal} bin between 18.6 and 20 GPa, more than 50% of the model runs show fault reactivation to distances beyond 8.3 m from the boundary. This indicates that with increasing E_{seal} the probability that fault reactivation will occur at a certain distance into the seal increases.

The strongest correlations are found for the Young's modulus in the seal, the friction parameters and the injection temperature. This can be well understood since larger moduli in the seal cause larger thermoelastic stresses in the seal, and the same holds for larger temperature differences. The friction parameters control how prone possible faults are to failure at given stress.

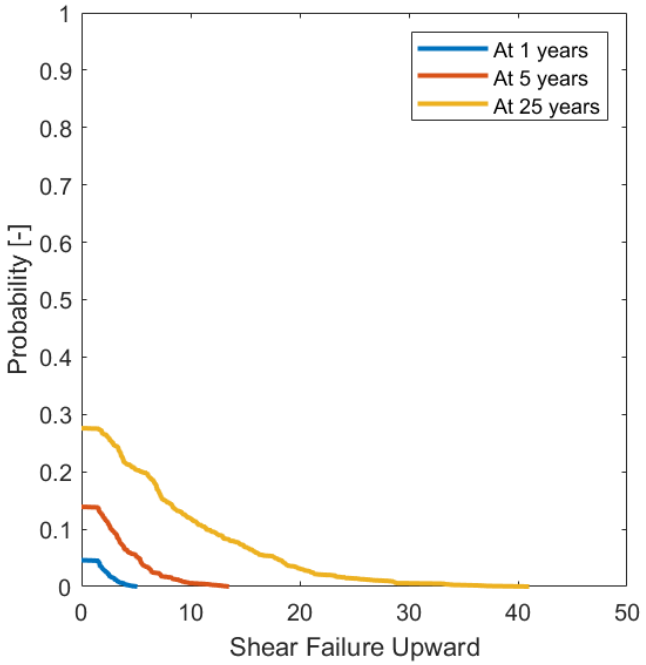

Figure 17 Probability of reactivating the seal upwards from the aquifer beyond the distances on the x-axis. Less than 30% show failure in the seal, even after 25 years.

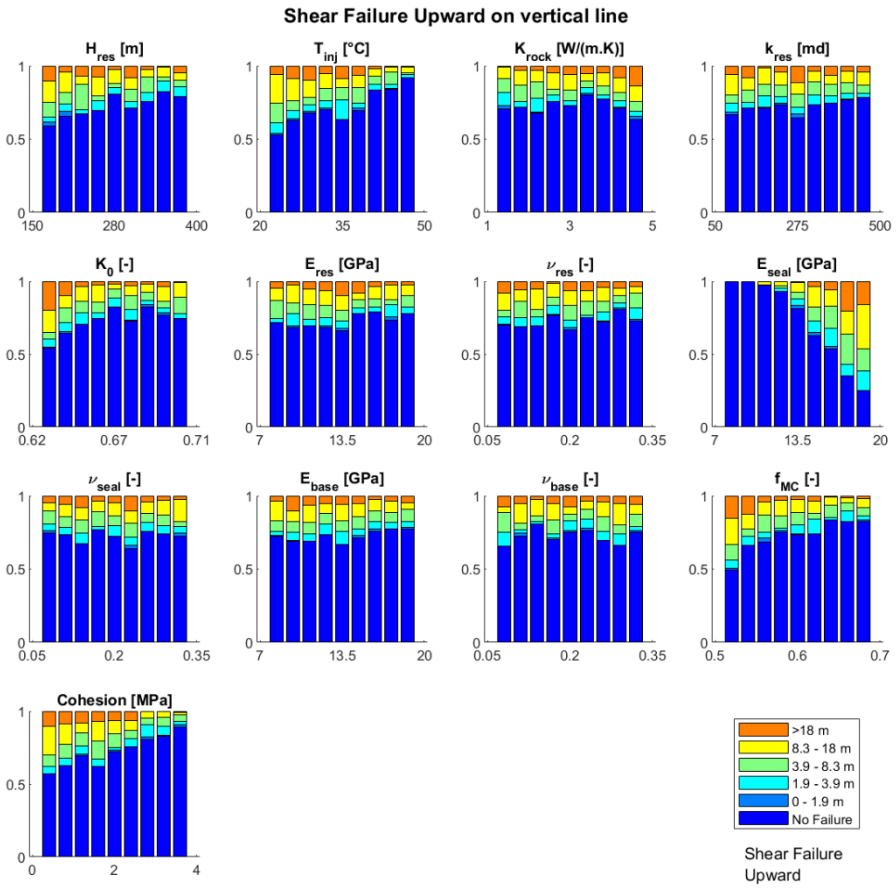

Figure 18 Distribution of the shear failure into the seal against variation of the uncertain parameters. The 13 subplots show the results according to a specific parameter: reservoir thickness (H_{res}), injection temperature (T_{inj}), rock thermal conductivity (K_{rock}), reservoir permeability (k_{res}), horizontal / vertical stress ratio (K_0), reservoir Young's modulus (E_{res}), reservoir Poisson ratio (ν_{res}), seal Young's modulus (E_{seal}), seal Poisson's ratio (ν_{seal}), base Young's modulus (E_{base}), base Poisson ratio (ν_{base}), Coulomb friction parameter (f_{MC}) and cohesion. For each input parameter shown in the subplots, the model runs have been grouped into 9 equally sized bins. Within each bin, the coloured bars indicate the fraction of model results within a certain range of upward shear failure. A correlation is found where the distribution of the sub-bins colours depends on the parameter bin values on the horizontal axes. The strongest correlations are found for the Young's modulus in the seal, the friction parameters and the injection temperature.

3.3.7 Stochastic analysis for calculations vs distance from the well

We now proceed to the results of the stochastic calculations on a horizontal line. These calculations were performed to assess the sensitivity of the extent and magnitude of induced stress changes and SCU to the input parameters and their uncertainties. Again, an ensemble of 1000 realizations was constructed based on the uncertainty of the parameters indicated in Table 1. The most critical depth for reactivation is close to the boundaries of the aquifer. Therefore we have taken a horizontal line at that depth, i.e. 10% of the aquifer thickness below its upper boundary.

A fault is considered to be reactivated if the Shear Capacity Utilization (SCU, Eq. 6) is larger than unity. For every ensemble member, a plot of SCU and the increase in Coulomb Failure

Function, ΔCFF, like those in Figure 8 and Figure 9 can be constructed. From these profiles we determine the largest distance between a fault and the injection well where SCU equals unity and the fault can be reactivated (r_{fault}) as a first measure for potential seismicity. We also determined the largest distance where ΔCFF is larger than 1 MPa ($r_{CFF\text{-}1MPa}$). The latter was quite intuitively chosen as a maximum radius of considerable induced stress changes. In principle, even small changes in the order of tidal influence on the stress can trigger a seismic event if the stress before geothermal injection is close to failure, therefore the usage of ΔCFF may be limited. Both measures are also compared with the radius of the cooled zone, which was determined as the distance where the temperature is the average between injection temperature and original aquifer temperature. Figure 19 and Figure 20 show the result.

Figure 19 (left) shows that the probabilities of criticality increase with time. After 1 year, only 20% of the cases show any criticality; this number increases with time, but remains smaller than 50% after 25 years. At the same time, more and more cases show criticality at larger distances. This increase is strongly correlated with the growth of the cooled zone (Figure 19 right). A clear step occurs at the cooled-zone radius: the number of cases with criticality at larger distances rapidly decreases.

The "maximum radius with considerable ΔCFF" also grows with time, and all cases show considerable ΔCFF within the cooled zone – hence the start of the curves at values slightly above unity in Figure 20 (right). Beyond that value the probabilities decrease, and for some cases a considerable ΔCFF can even be reached at 3 times the cooled-zone radius after 1 year; decreasing to less than 2.5 times after 25 years.

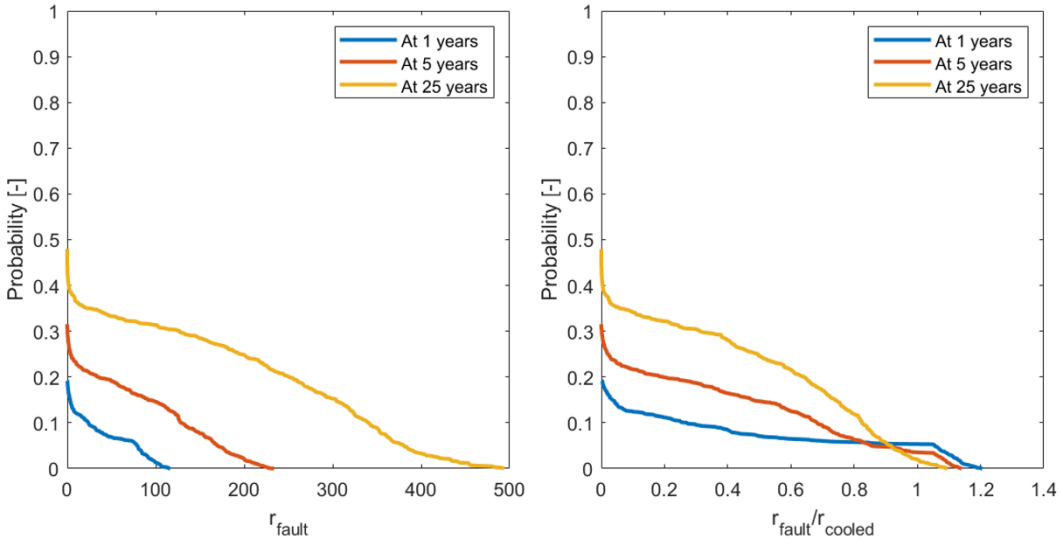

Figure 19 Probability of finding $SCU > 1$ at given distances to a fault (left) and at the relative distance (right). For distances larger than 1.2 times the cooled-zone radius, the stress is non-critical for all the cases.

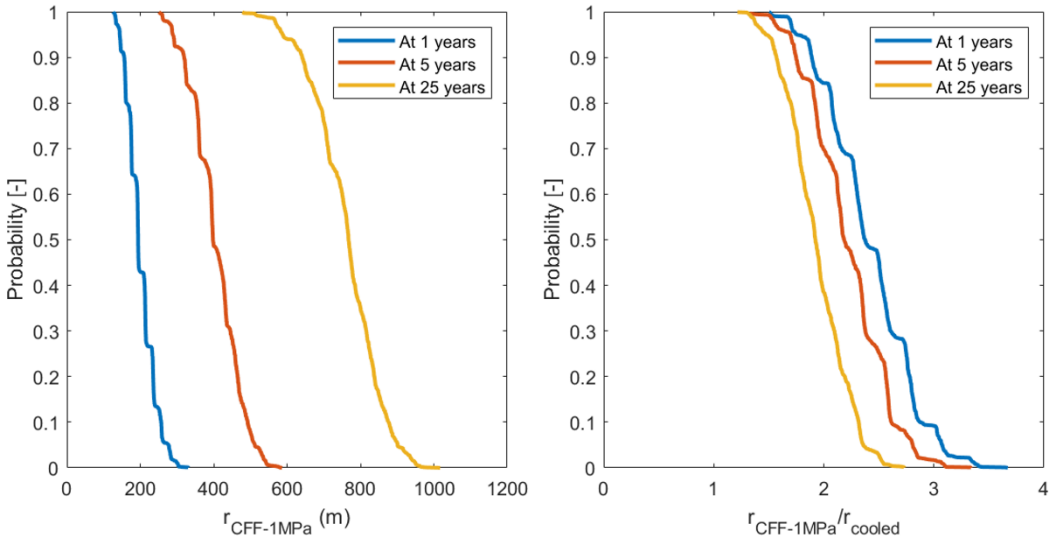

Figure 20 Probability of finding considerable ΔCFF at the given distance to the well (left) and at the relative distance (right). All cases experience considerable ΔCFF within the cooled zone. Considerable ΔCFF can occur up to 3 times the cooled-zone radius after a year, decreasing to 2.5 times the cooled-zone radius after 25 years.

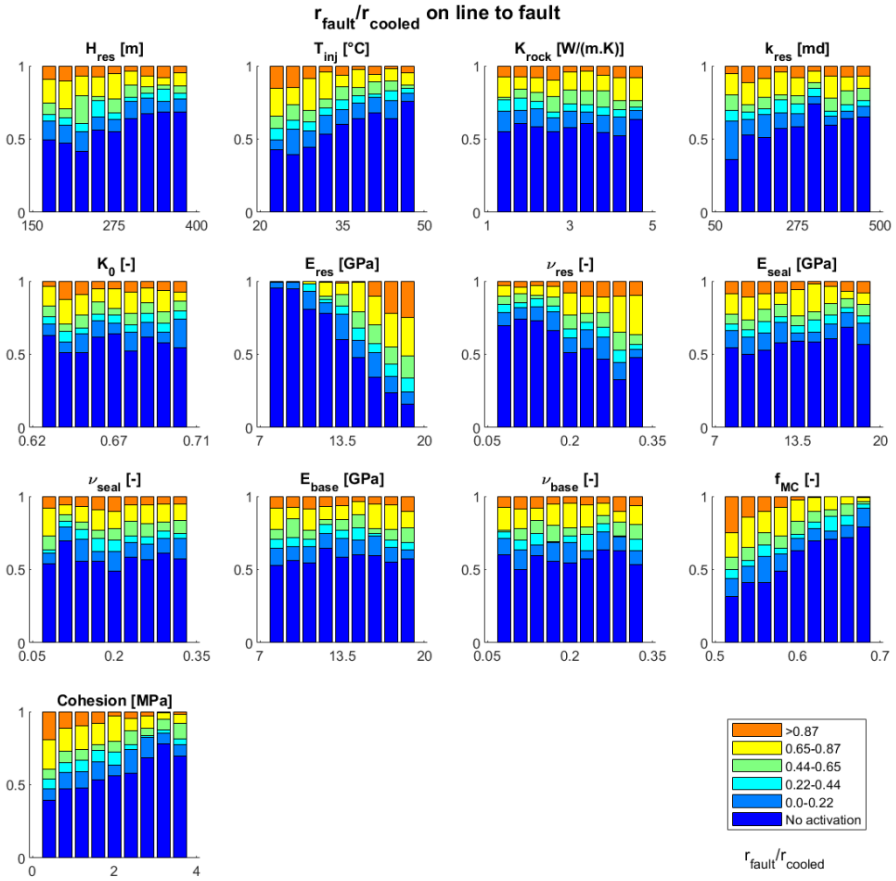

Figure 21 Distribution of the relative radius of criticality against variation of the uncertain parameters. Input values are in the bins on the horizontal axes of the subplots; the resulting values for these values are

ordered in coloured sub-bins ranging from small to high values. A correlation is found where the colour distribution of the sub-bins is depends on the parameter bin values on the horizontal axes. See for a discussion the main text in the report.

Now the question is appropriate which are the most important uncertainties and what is their influence. This is investigated by comparing the outcome of the calculations with the input parameters. We present the analysis for the relative fault distance for criticality and for the relative maximum radius of considerable ΔCFF in Figure 21 and Figure 22. In these figures we have ranked the results against the uncertain parameters, similar to the analysis in Figure 18. First, the measure that is investigated (r_{fault}/r_{cooled}; $r_{CFF\text{-}1MPa}/r_{cooled}$) has been determined for each ensemble member. Then, for each input parameter that was varied in the stochastic analysis the results were binned in 9 bins, spanning the full range between the minimum and maximum value of the parameter that was explored in the stochastic analysis. Per bin, the normalized fraction of model results for a certain value of the evaluation measure are indicated with the different colors.

For the fault distance for criticality (Figure 21) we firstly see a clear correlation with the geomechanical parameters of the aquifer. A larger elastic modulus, larger Poisson ratio and a smaller stress ratio all increase the probability of a large critical radius considerably. The probability of finding larger critical radii is also increased by more critical friction parameters: smaller Mohr-Coulomb friction coefficient or smaller cohesion. Finally, a smaller injection temperature and associated larger thermoelastic stresses increase the probability of finding larger critical radii.

A slightly different picture evolves from the analysis of relative maximum considerable ΔCFF. The friction parameters here have no influence, which is understood because they are not part of the calculation of ΔCFF. Injection temperature, elastic modulus and stress ratio have similar effect as they have on the radius of criticality. Noteworthy here is the influence of the aquifer thickness. Larger thicknesses increase the probability of finding larger values for ΔCFF. This is related to the height / radius ratio of the cooled zone. The effect is not seen in the radius of criticality since it is often closer to the cooled-zone radius, which decreases the effect of the thickness of the cooled zone.

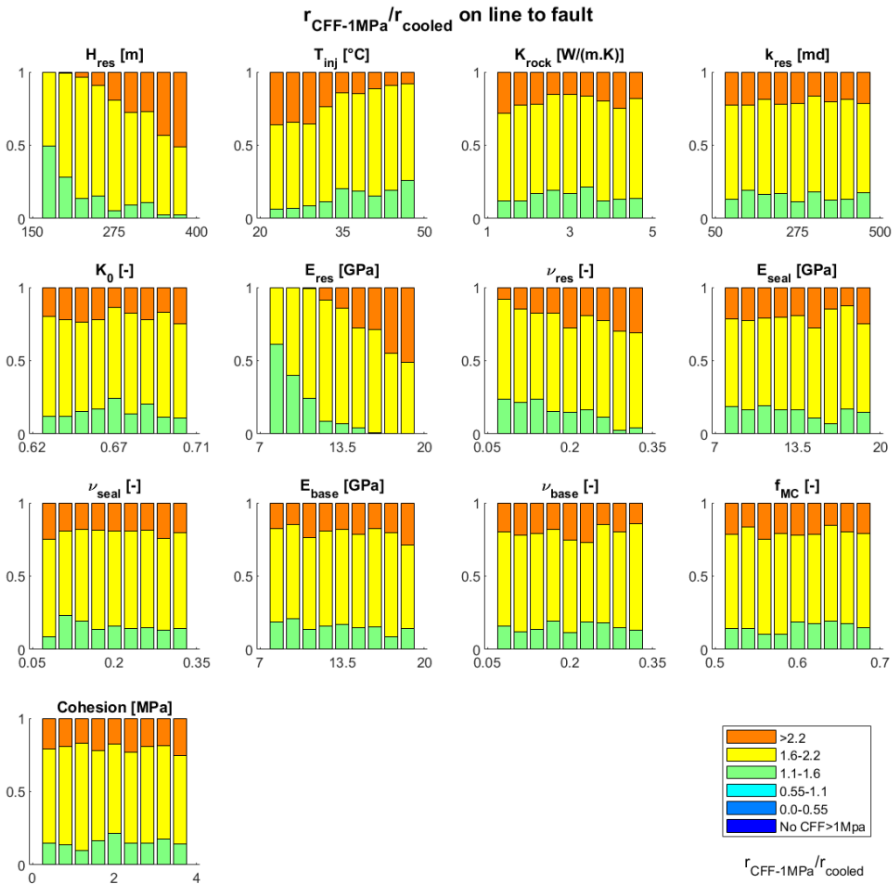

Figure 22 Distribution of the relative radius of considerable ΔCFF against variation of the uncertain parameters. Input values are in the bins on the horizontal axes of the subplots; the resulting values for these values are ordered in coloured sub-bins ranging from small to high values. A correlation is found where the distribution of the coloured sub-bins is depends on the parameter bin values on the horizontal axes. See for a discussion the main text in the report.

3.4 PANTHER

The PANTHER cases deploy the same subsurface parameters as the SRIMA cases. Only the geometry is different: while SRIMA uses radial symmetry, in PANTHER plane-strain conditions are utilized (no strain in the out-of-plane direction). PANTHER has been developed to model the effect of a depleting or cooling reservoir on the stresses and the Shear Capacity Utilization (SCU) of a fault, while the fault offsets the reservoir parts on either side (Figure 23).
We investigate the effect of both pressure depletion and cooling. While the pressure changes due to injection are relatively small with respect to the typical depletions already experienced due to the earlier depletion, and localized in the direct vicinity of the injection well, the effect of the pressure difference with the bounding layers due to depletion is significant. In addition, the distinction is important between cases where seal and base are subject to pressure diffusion or not. Cooling is applied uniformly over the reservoir, with thermal diffusion to the seal and base. We used a value of 10 MPa pore pressure reduction with respect to virgin conditions and 55°C temperature reduction.

PANTHER models a cross section of a reservoir, with a fault dipping under an angle θ and having an offset between the footwall and the hanging wall. Our focus is on the effect of the offset because this cannot be modelled in SRIMA. With respect to the SRIMA simulations, the offset has only an effect if it introduces a distortion of the stress fields with respect to the case without offset – which is only the case when there are pressure or temperature differences with respect to the bounding layers. Therefore, the simplification to the 2D geometry is warranted for this study: it mimics the situation of a fault well within the distorted temperature or pressure field. Besides the effect of the offset for a critical dip angle, we also evaluate the effect of the dip angle itself, and the relationship between the two.

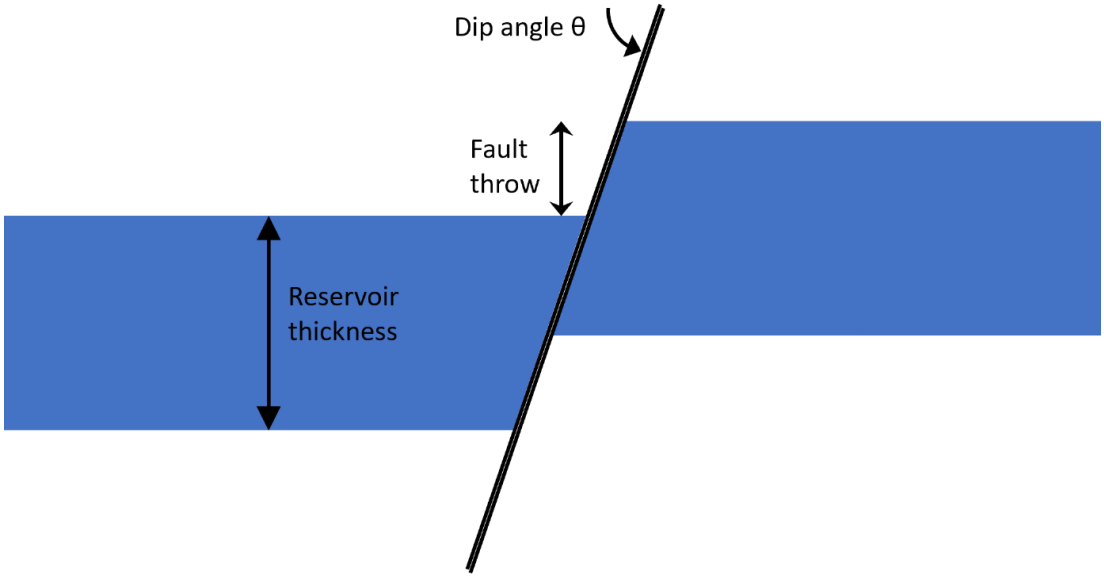

Figure 23 Geometry of PANTHER simulations. The picture show a situation with positive offset: the hanging wall is deeper than the footwall

A typical result is provided in Figure 24. The stresses are calculated for a 300 m thick reservoir that is cut in two parts by a 60° dipping fault with a throw of 150 m. The center depth is 3150 m; the two parts of the aquifer are assumed unbounded in the direction away from the fault. Thermal diffusion into the bounding layers causes a smoothing of the induced thermo-elastic stresses; pressure diffusion is not taken into account in this simulation and the lower pressure in the aquifer results in stress concentration at the upper and lower boundaries of the two parts of the aquifer. When slip is allowed to reduce the shear stress to the Mohr-Coulomb failure envelope, the SCU is maximized on unity and some slip develops in that zone.
We now proceed to discussing some of the sensitivities that we studied. Figure 25 demonstrates the effect of depletion without diffusion, for a range of values for the fault throw. We see the stress concentrations at the four boundary levels of the two sides of the aquifer. The largest effect of the fault throw is when the throw equals the aquifer thickness, i.e. when the upper boundary of the hanging wall is at the same depth as the lower boundary of the footwall. Hydraulic diffusion removes the stress concentrations, but the global behavior is maintained (Figure 26). Cooling (Figure 27) has a similar effect as depressurization on the total stresses – however, fault reactivation is controlled by the effective stresses. As a result, we see a decrease of the effective normal stress working on the fault in the middle of the zone for the thermal cooling case, while we see an increase in effective normal stress for the depressurization case. Furthermore, the magnitude of the induced stresses and the SCU by cooling are larger than those by depressurization for this case.

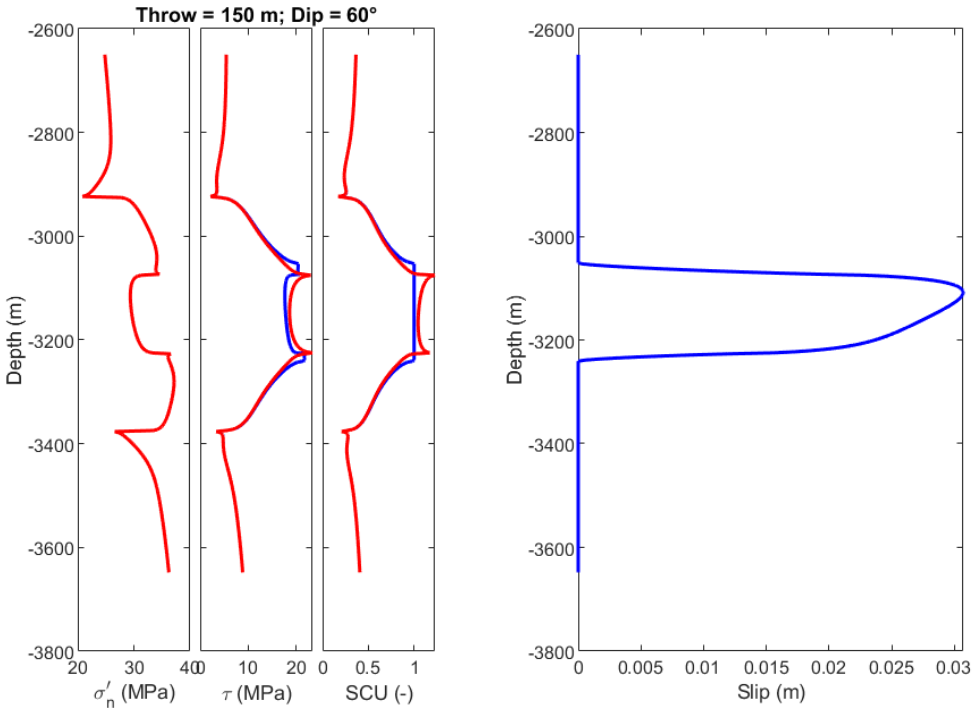

Figure 24 Typical example of stresses and SCU (left) and slip (right) calculated on a fault that is dipping with 60° and offset with 150 m. Effects of temperature and pressure are included; no pressure diffusion into the bounding layers is assumed. Red curves: no slip calculated (purely elastic); blue curves: slip is allowed to happen and to relax the stress down to $SCU = 1$.

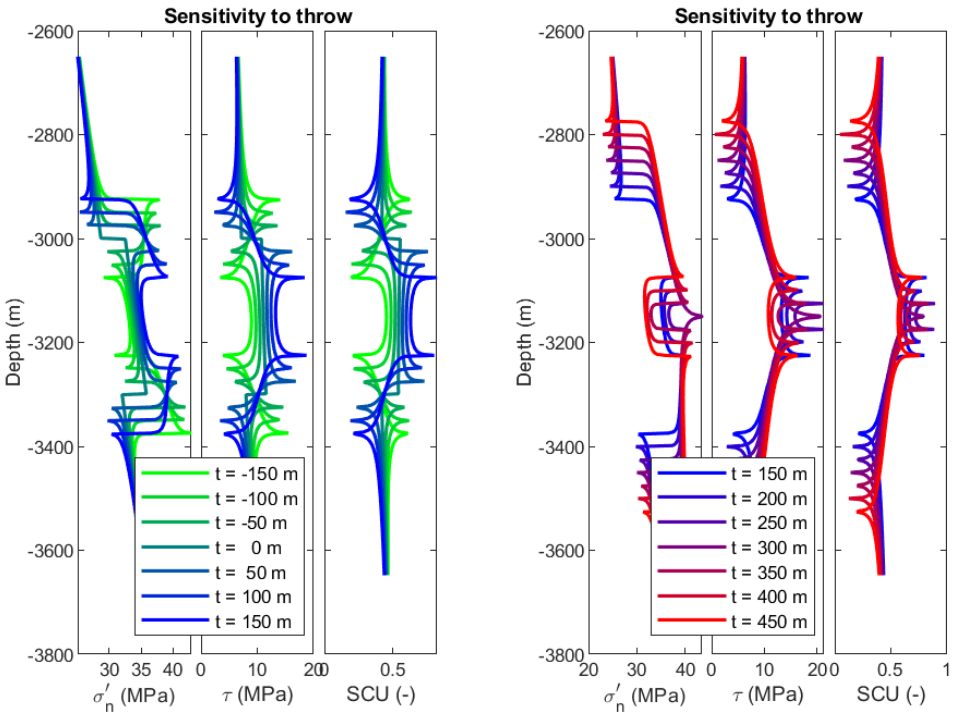

Figure 25 Simulations of normal effective stresses, shear stresses and SCU for 10 MPa reservoir depletion without diffusion. Left: fault offsets between -150 m (reverse displacement) and 150 m (normal displacement). Right: normal fault offsets between 150 m and 450 m.

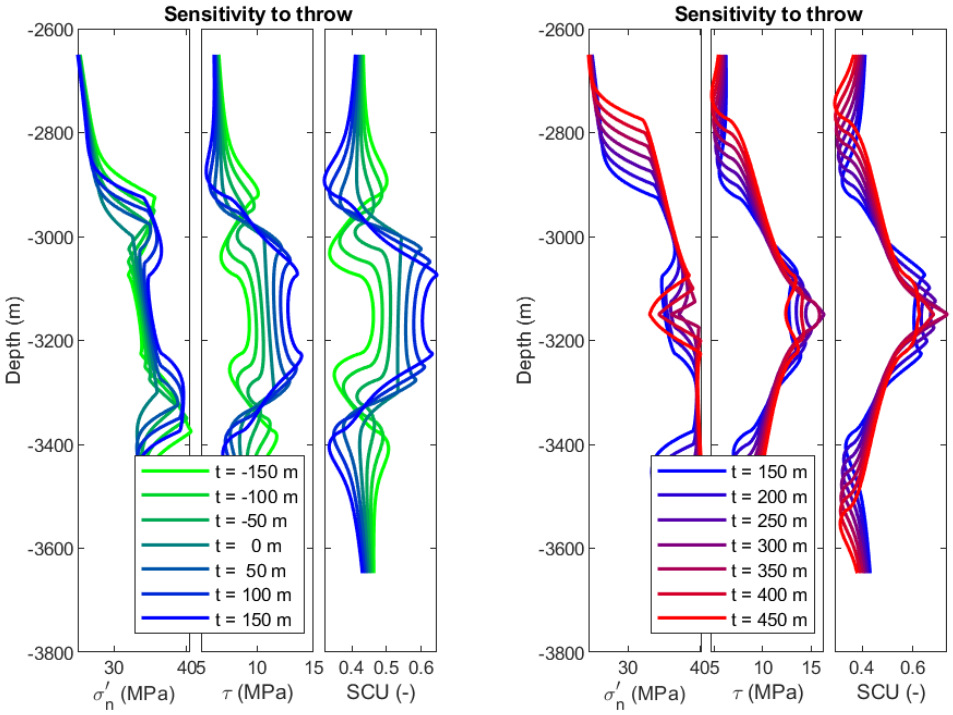

Figure 26 Simulations for reservoir depletion with diffusion, after 25 years, Same identification of curves as in Figure 25.

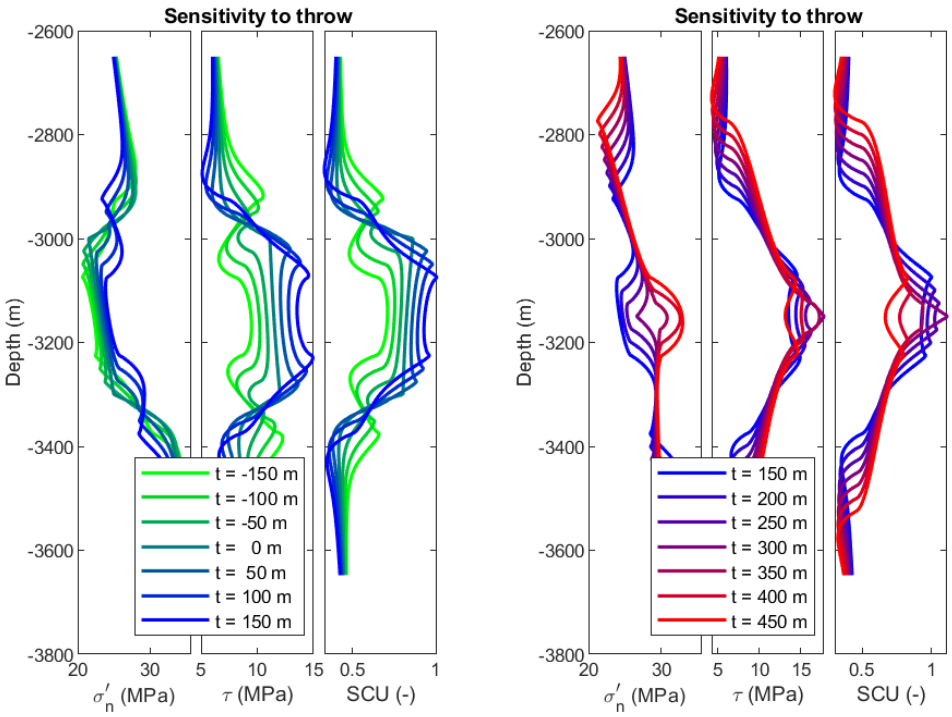

Figure 27 Simulations for 55°C reservoir cooling for 25 years, Same identification of curves as in Figure 25.

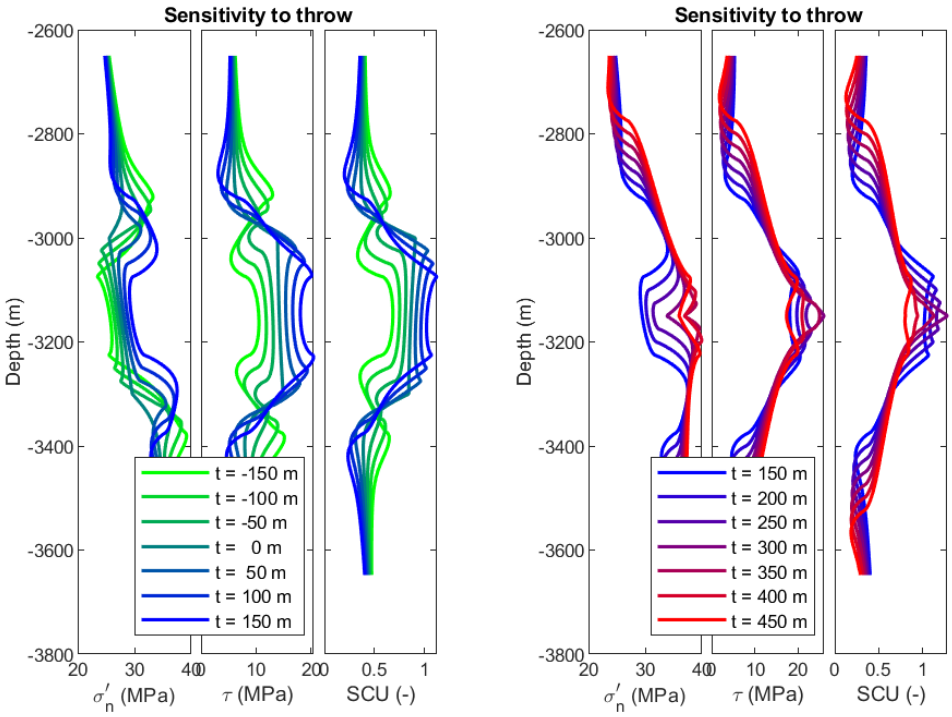

Figure 28 Simulations for 25 years combined reservoir depletion (10 MPa reduction) and cooling (55°C temperature decrease). Same identification of curves as in Figure 25.

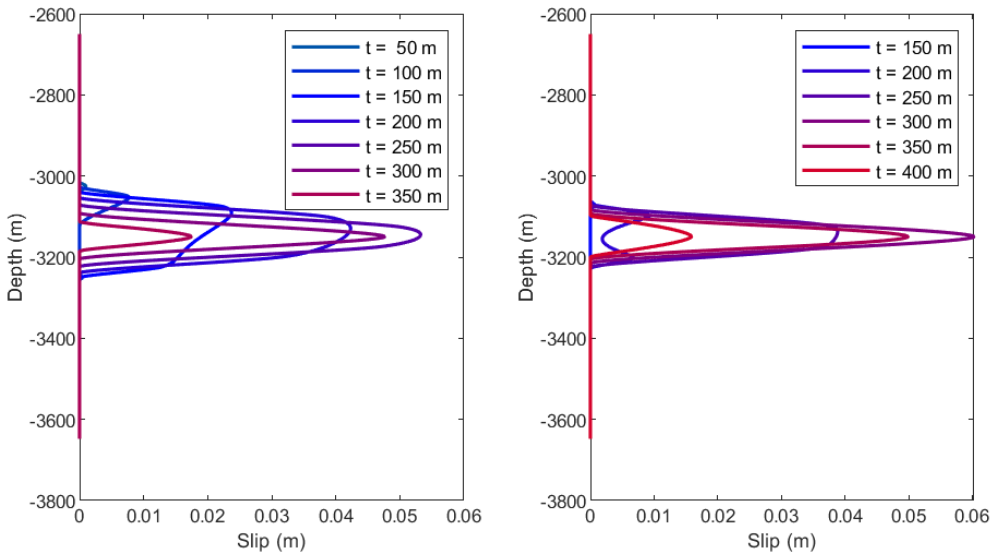

Figure 29 Slip for combined depletion and cooling of the aquifer . Left: 60° dip. Right: 80° dip. Only those cases are shown that exceed the reactivation criterion ($SCU > 1$) and consequently show slip.

The combined effect of depletion and cooling is presented in Figure 28. Generally speaking, SCU is increased between the upper boundary of the upper aquifer and the lower boundary of the lower aquifer, i.e. over most of the depths where a pressure or temperature disturbance is present. When compared to zero offset, negative offsets (the hanging wall being shallower than the footwall) cause smaller increase of SCU; positive offsets (normal displacement with the hanging wall deeper than the footwall) cause a larger increase of SCU in the region where the aquifer intervals overlap. The maximum values for SCU occur for an offset equal to the aquifer thickness (i.e. 300 m), at the depth where the upper boundary of the hanging wall touches the lower boundary of the footwall. We see that for a throw between 50 and 400 m, the SCU exceeds unity. When the slip calculation option is enabled, we observe (Figure 29, left) that slip takes place mainly at the upper boundary of the hanging wall when the throw is small; it becomes larger for larger throws and reduces again when the two reservoir parts do not overlap anymore.

The stress response on the fault depends heavily on the fault dip. Figure 30 shows the fault stresses and resulting SCU for faults dipping at 40° and 80°, respectively. While the absolute values for the smaller dip of 40° decrease and slip conditions are not reached, values for the 80° dip remain high and cause reactivation. Figure 29 (right) shows how the slip values for the 80° dip compare to the 60° dip base case: they are slightly less, and more concentrated in the centre of the fault zone.

This dip angle dependency is further explored in Figure 31. The figures show the elastic responses to pressurization and cooling for dips ranging between 30° and 90°, for fault throws of 0, 150, and 300 m. The cases with throws of 150 and 300 m and dips near to the critical angle show SCU exceeding unity and consequently slip when that option is enabled. Most slip is observed for the case where the throw equals the aquifer thickness and the upper boundary of the hanging wall touches the lower boundary of the footwall (Figure 32).

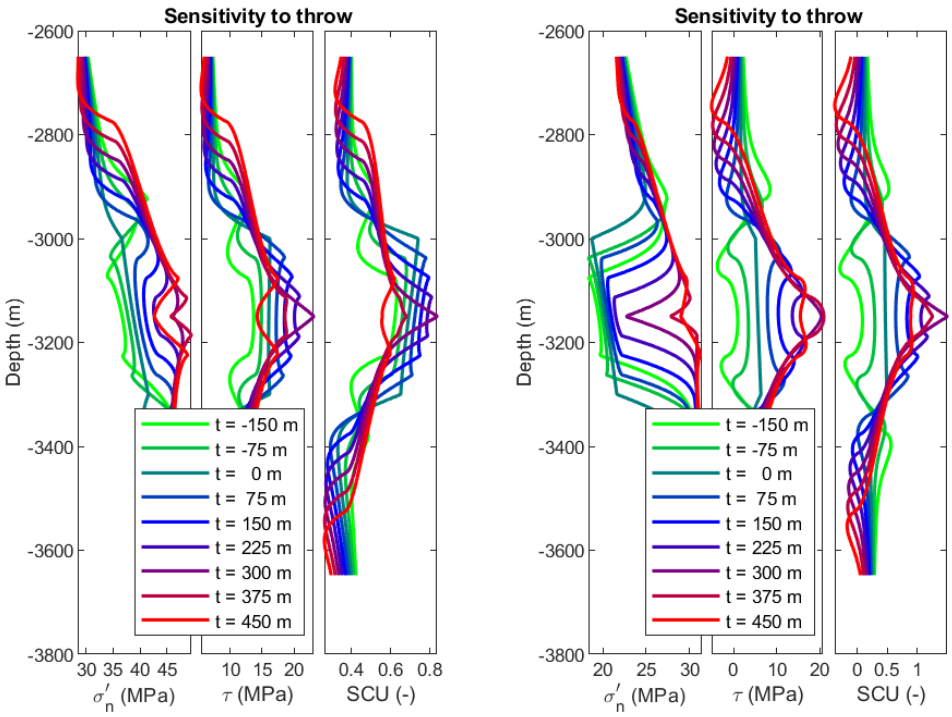

Figure 30 Simulations for 25 years combined depletion and cooling. Left: 40° dip. Right: 80° dip

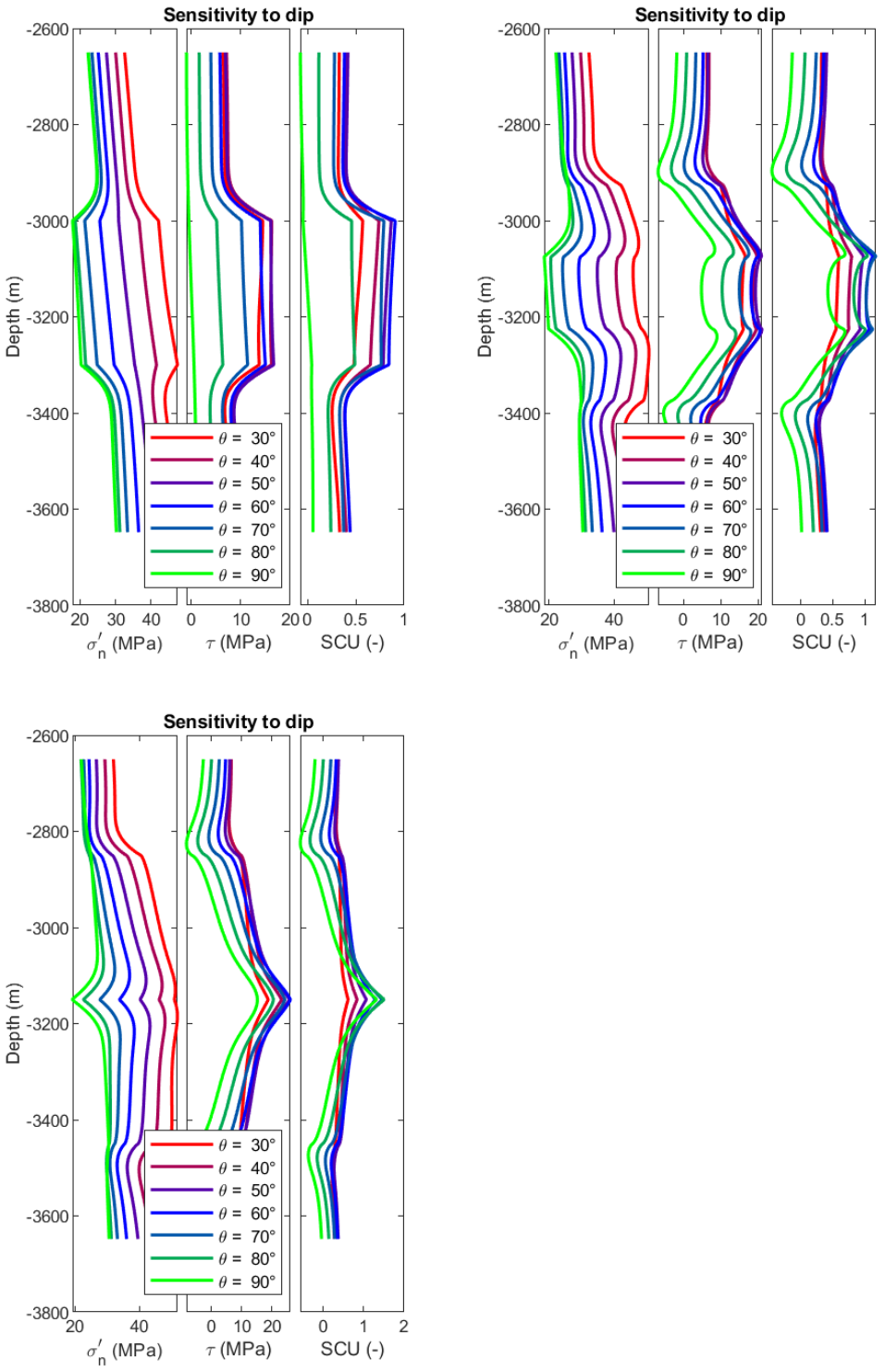

Figure 31 Simulations for 25 years combined depletion and cooling with different dip. Throw is 0 m (top left); 150 m (top right); 300 m (bottom).

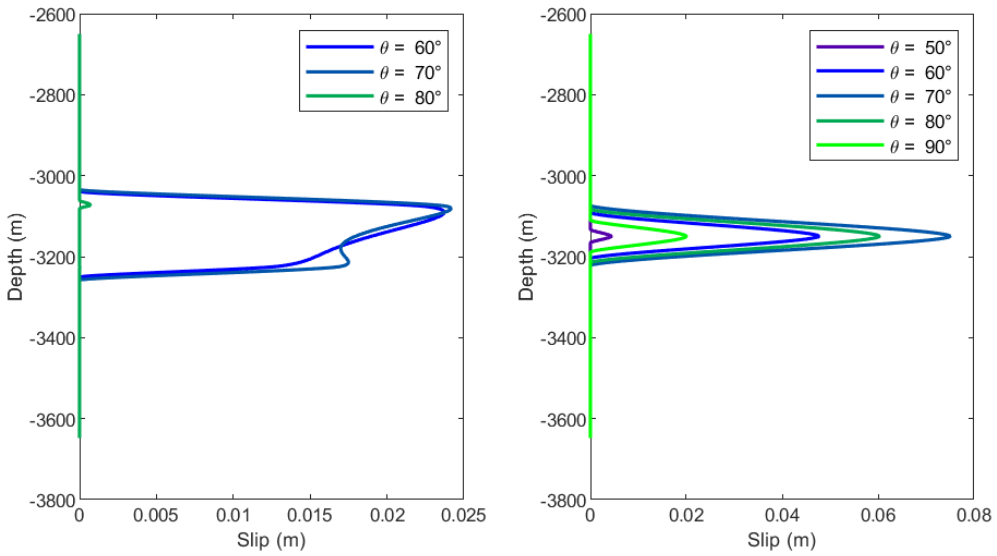

Figure 32 Slip for simulations with different dip. Left: throw = 150 m. Right: throw = 300 m

From the PANTHER analysis we conclude that it is important to assess the offset of a fault when it is present in the cooled or depressurized zone of a geothermal field. An offset equal to the aquifer thickness, with the top of the hanging wall at the same depth as the bottom of the footwall, increases the effect of depletion and cooling on the induced stresses. This is the case for the complete range of values for the dip of the fault. The offset of the aquifer depth at the two sides of a fault therefore constitutes an important parameter in the analysis of potential seismicity. It can considerably increase the probability of failure.
Depletion of the aquifer has a negative effect on SCU for the low values of Poisson ratio and the high values for the poro-elastic constant that we deployed. Aquifer depletion brings faults closer to the critical value. This is in line with the results obtained with SRIMA above (Figure 3 and Figure 9). The introduction of a fault offset amplifies the effect of the depletion. This is visualized in Figure 28 and Figure 29. It introduces stress concentrations at the upper and lower boundaries of the aquifer. These peaks are relieved when pressure diffusion into seal and base is incorporated, but the overall effect of offset on the stresses does not disappear. The total effect is demonstrated in Figure 24.

3.5 Concluding remarks

We have investigated the impact of a typical geothermal operation in the SW aquifer, where pressure depletion had earlier taken place due to equilibration with the depleted gas fields connected to it. A typical geothermal operation involves the construction of a well doublet, with long-term injection of cold water in the injection well. This injection causes a local pressure increase and a propagating cooled volume around the injector. Both the increase of the pressure and the decrease of the temperature induce stress changes, and thereby change the probability of reactivating pre-existing faults. In the case of seismic fault reactivation this would translate into a change in probability of seismicity in the area. It was the objective of the present study to make first-order estimates of these effects.
An important observation is that the temperature development during geothermal operations initiates effects that are different in character from the effects of the pressure depletion that happened prior to geothermal injection. The changes in total stress are similar, because the poro-elastic and thermo-elastic additions to the elastic response in the constitutive equation are identical in character. However, seismicity is controlled by the effective stress, i.e. the

difference between total stress and pore pressure. Figure 3 presents the two effects in a Mohr diagram: pressure and temperature changes cause a movement of the stress that works on a fault plane in different directions. A treatment of temperature effects that is separate from pressure effects is required.

The main thermo-elastic effects are happening in the cooled zone of the aquifer and around it, up to 1.5 times the radius of the cooled zone. Reactivation of faults is also mainly concentrated in this region. Therefore it is important to map both the cooled volume and the geometry of faults that may be seismogenic. The radius of the cooled reservoir volume depends on the volume of injected cold water, the height of the permeable zone and the thermal properties of the fluid and the rock. It is possible to monitor the propagation of the cooled zone with well testing and with pulse tests (Fokker, P. A. et al. (2021)). Distributed temperature sensing (DTS) in nearby wells can also be very helpful, as was demonstrated by Dinkelman et al. (2022). For the characterization of fault locations and geometries, common geological and geophysical methods are available and need to be deployed; we refer to earlier Chapters of this report, where we performed these investigations for the current study.

A fault that offsets the two adjacent parts of the aquifer shows different seismogenic response than a fault without offset. For a fault with normal displacement, the increase in Coulomb Failure Function (ΔCFF) and associated Shear Capacity Utilization (SCU) in the reservoir are larger than for zero offset. This effect is at its maximum when the top of the hanging wall is at the same depth as the bottom of the footwall. The effect is, however, only present in the cooled or pressurized part of the aquifer. Depletion of the aquifer in combination with a fault offset increases SCU, because additional stress concentrations are generated at the top and bottom interfaces of the two aquifer parts at the location of the fault. Faults with a considerable offset that are located within the projected cooled region around an injection well therefore pose an additional threat to geothermal operations and should be investigated individually. From the present study, an offset of less than 1/3 of the layer thickness seems to be on the safe side.

The stresses at the start of possible geothermal operations in the SW Aquifer depend on both the virgin stresses and on the depletion due to pressure equilibration with the surrounding gas reservoirs, which has been studied above. Non-depleted parts of the aquifer can therefore be considered slightly more stable and less seismogenic. This balance, however, depends on the parameters chosen. As an example, higher Poisson's ratio and lower poro-elastic constant reverse the destabilization tendency of depletion to a stabilizing tendency.

The effect of injection rate is not expected to be large within the range of expected permeabilities and projected rates of injection. The contribution of the pressure increase due to the Darcy flow in the aquifer is moderate, as was shown by the limited sensitivity of the results to permeability (Figure 18, Figure 21 and Figure 22). Indeed, reducing permeability has a similar effect on the pressure change as increasing the injection rate. The largest effect of the injection rate will be by the associated size of the cooled zone. The volume of cooled rock is linearly dependent on the volume of injected cold water, and hence on the duration of the injection operations. In the same way, the thickness also affects the size of the cooled zone. However, the effect of thickness is magnified by the influence of the vertical / horizontal dimension ratio on the induced stresses: thicker zones result in less critical stresses.

There is still considerable uncertainty on a number of the key input parameters: virgin stresses, fault frictional properties, elastic moduli. These uncertainties propagate into an uncertainty in the expected stress changes, including the increase in Coulomb Failure Function and the Shear Capacity Utilization. A prior analysis of potential geothermal operations always needs to take into account these uncertainties. A general conclusion of this study is that the radius inside which stress changes are considerable is limited to 1.5 times the radius of the cooled zone, for which a good estimate can be given by Eq. (8).

4 General discussion and conclusions

The work performed here focusses on the impact of potential geothermal operations in the SW aquifer of the Groningen gas field. The research questions are aimed at generic questions relevant for all operations in this area. Consequently, the work has focused on generic results that are broadly applicable to all potential geothermal projects. This also means that the results of this work are not sufficiently project-specific to serve as direct input to an SHRA for a particular operation. However, due to their broad applicability, the results from this project can serve as important input to such an SHRA.

The *seismicity propensity* map in Chapter 2 shows that, regardless of project design, there are areas that are more and less prone to seismicity under the same loading. This does not imply that projects cannot be safely executed in the high propensity areas, nor that projects in the low propensity area cannot generate significant seismicity. It does however mean that, given a certain project design, the expectation is that that same project will lead to more seismicity in some areas than in others. This is relevant information for both individual geothermal projects, who may or may not have a degree of flexibility in the planning of their location, and for governmental and regulatory bodies who may be interested in the spatial and temporal planning of several geothermal projects. The calculations in Chapter 2 are based on the assumption that the assumptions behind the Groningen seismic source model, which was developed for dealing with pressure changes, remain valid in the context of temperature changes. Specifically, a given amount of vertical strain leads to the same stress change ΔC, regardless of whether the vertical strain is caused by a pore pressure change or temperature change. This is due to the 'amplification' of stresses at offset faults (see Bourne and Oates 2017 for details) in the simplified 'thin-sheet' geometry. Note that in the analyses in Chapter 3, stresses are computed along faults while taking into account a more complex geometry. In these models, temperature changes lead to a different stress path than pore pressure changes and can no longer be converted into an equivalent pore pressure change by using vertical strain as an intermediate quantity. In the context of assessing regional seismicity propensity, we argue that using the best available seismic source model for the region (i.e. the Groningen seismic source model) is a sensible choice, and hence we can use the equivalence between pore pressure and temperature changes in this context. In the context of assessing the stress impact of potential geothermal operations in terms of their extent and magnitude, we believe the tools applied in Chapter 3 are better suited.

In Chapter 2, we further assume that the induced strains are primarily uniaxial in nature, which is a sensible assumption in the context of pore pressure-induced strains in a laterally extensive, highly permeable reservoir, remains true for geothermal operations. Although strains induced by typical geothermal operations are less uniaxial in nature, due to their relatively large spatial temperature gradients, we believe that for a first-order assessment of seismicity propensity, the chosen approach is sensible and valid. We are investigating *seismicity propensity,* which can be seen as an expression of the probability of encountering faults that are near failure and only need a small stress disturbance for failure to occur. In the case of the SW aquifer of the Groningen field, to what extent faults are near failure is determined by their stress history, which is (up to now) determined by pressure depletion. In

other words, although the uniaxial strain assumption may not be fully valid for modelling the stress disturbance caused by geothermal operations, it is a valid assumption to describe the stress history of the faults, and therefore of their propensity for failure and seismicity.

The work presented in Chapter 3, on the extent and magnitude of stress changes induced by the geothermal project, contains valuable input for any geothermal project. The main geomechanical effects of interest are related to the injection well. Although the spatial extent of influence and the magnitude of the stress changes depend on the local mechanical parameters and the project specifications, the result that the main effects are closely tied to the cooled zone is generally valid. Similarly, the result that pressure depletion prior to commencing geothermal operations leads to less stable or more seismogenic circumstances applies in general and is useful to consider during project design.

The main conclusions of this report can be summarized as follows:

- The area with the highest seismicity propensity is just north of the city of Groningen and does not change its position through time. It's closely related to the pore pressure depletion in the Bedum gas field (Figure 1).
- The main thermo-elastic effects are associated with the cooled volume of the aquifer centered around the injector, reaching up to 1.5 times the radius of the cooled zone. Reactivation of faults is also mainly concentrated in this region.
- Poro-elastic effects depend on injection rate, permeability and thickness of the injection layer. However, the uncertainties and operational boundaries of these numbers make their effects generally less important than thermoelastic effects in the context of the SW aquifer.
- For a project-specific seismicity study, it is important to map both the cooled zone and the geometry of faults that may be seismogenic. We suggested methods to monitor the cooled reservoir volume, including well testing, pulse testing and DTS.
- It is important to assess the offset of a fault when it is present in the cooled or depressurized zone of a geothermal field. An offset equal to the aquifer thickness, with the top of the hanging wall at the same depth as the bottom of the footwall, maximizes the effect of depletion and cooling on the induced stresses. This is the case for the complete range of values for the dip of the fault. Non-depleted parts of the aquifer are typically slightly more stable and less seismogenic. However, this does depend on the geomechanical parameters chosen (specifically on the Poisson's ratio and poro-elastic constant), and on the presence of faults with offset.
- Uncertainties in input parameters are important to consider and should be taken into account in any project-specific analysis of geothermal operations. A number of key inputs have been identified in this study: virgin in-situ stress state, fault frictional properties, elastic moduli.

References

Bakx, E., Buijze, L., & Wassing, B. B. T. (2022). Formation, lithology and region-specific stress field in the Netherlands. TNO Utrecht.

Buijze, L., Fokker, P. A., & Wassing, B. B. T. (2022). Quantification of induced seismicity potential of geothermal operations: Analytical and numerical model approaches. TNO Utrecht.

Buijze, L., Veldkamp, H., & Wassing, B. (2023). Comparison of hydrocarbon and geothermal energy production in the Netherlands: reservoir characteristics, pressure and temperature changes, and implications for fault reactivation. Netherlands Journal of Geosciences, *102*, e7.

Dinkelman, D., Carpentier, S. F. A., Koenen, M., Oerlemans, P., Godschalk, B., Peters, E., Van Wees, J. D. A. M.High temperature aquifer thermal energy storage performance in middenmeer, the netherlands: Thermal monitoring and model calibration. 17-21 October 2022

Fokker, P. A., Salina Borello, E., Viberti, D., Verga, F., & Van Wees, J. D. (2021). Pulse testing for monitoring the thermal front in aquifer thermal energy storage. Geothermics, *89* doi:10.1016/j.geothermics.2020.101942

Fokker, P. A., Buijze, L., & Pluymaekers, M. P. D. (2023). SRIMA: Background Information of Python tool.

Fokker, P. A., & Wassing, B. B. T.A fast model for THM processes in geothermal applications. 11-14 June 2019

KEM-19b. Evaluation of post-abandonment fluid migration and seismic hazard assessment in the South-West aquifer of Groningen. TNO 2025 R10452

KEM 24-b. Preliminary assessment of beneficial effects of nitrogen injection in depleted reservoirs. TNO 2024 R11366

Mathur, B., Hofmann, H., Cacace, M., Hutka, G. A., & Zang, A. (2024). Thermo-hydro-mechanical simulation of cooling-induced fault reactivation in Dutch geothermal reservoirs. Netherlands Journal of Geosciences, *103*, e1.

Nield, D. A., & Bejan, A. (2006). *Convection in porous media* Springer.

Pijnenburg, R. P. J., Verberne, B. A., Hangx, S. J. T., & Spiers, C. J. (2018). Deformation Behavior of Sandstones From the Seismogenic Groningen Gas Field: Role of Inelastic Versus Elastic Mechanisms. Journal of Geophysical Research: Solid Earth, *123*(7), 5532-5558. doi:10.1029/2018JB015673

Signature

TNO › Energy & Materials Transition › Utrecht, 7 July 2025

Energy & Materials Transition

Princetonlaan 6
3584 CB Utrecht
www.tno.nl

TNO innovation for life